The Abdus Salam
International Centre for Theoretical Physics

United Nations
Educational, Scientific and
Cultural Organization

IAEA
International Atomic Energy Agency

1965-29

9th Workshop on Three-Dimensional Modelling of Seismic Waves Generation, Propagation and their Inversion

22 September - 4 October, 2008

Achievements of strong motion seismology and its future directions

Kojiro Irikura
Aichi Institute of Technology and Kyoto University
Japan

irikura@geor.or.jp

The Abdus Salam International Centre for Theoretical Physics
2 September – 4 October 2008

9th Workshop on 3-D Modeling of Seismic Waves Generation, Propagation and their Inversion

Achievements of Strong Motion Seismology and its Future Directions

Kojiro Irikura (Aichi Institute of Technology and Kyoto University)

Contents:

Preface

Strong motion prediction has been progressed for promoting earthquake countermeasures learning from severe disasters of the 1995 Kobe earthquake in Japan. We have been developing the procedures of fault modeling for the prediction of strong ground motion as a recipe combining the active fault information with scaling relations of fault parameters from the waveform inversion of source processes using strong ground motions.

Validity of the methodology has been examined by comparing observed ground motions with synthesized ones estimated using the “recipe”. This technique was introduced to the “Regulatory Guide for Aseismic Design of Nuclear Power Reactor Facilities” revised in 2006 by the Nuclear Safety Commission of Japan. The 2007 Chuetsu-oki earthquake happened very close to the Kasiwazaki-Kariwa Nuclear Power Plant. The active faults caused to the earthquake have not been specified for the aseismic design of the plant. Through many investigations made after the earthquake we found that ground motions from the earthquake predictable as long as the source fault is specified through investigation of active folds and faults. Further improvements of the fault modeling are required to make more reliable evaluation of ground motions for earthquake safety designs.

Here I describe the theoretical backgrounds of the procedure for predicting strong ground motions, verification and applicability of the recipe” and overviews of strong motion seismology through recent work with my colleagues and myself. This note consists of five chapters. Chapter 1 describes methodology for predicting strong ground motions, so-called “Recipe”. Chapter 2 gives new developments of strong ground motion prediction learning from recent disastrous earthquakes. Here is shown validity of strong motion prediction recipe for inland-crust earthquakes. Chapter 3 shows source modeling and strong ground motion simulation of the 2007 Niigata earthquakes. The source model is successfully constructed using the empirical Green’s functions. The model was verified comparing ground motions observed during the mainshock with those simulated with the 3-D finite difference computation for realistic underground structures. Chapter 4 shows construction of long-period structure during subduction earthquakes using the three-dimensional finite difference method. In Chapter 4 long period ground motions in Osaka basin were numerically calculated from great subduction-zone earthquakes occurring along the Nankai Trough.

Chapter 5 shows damage prediction of long-period structure due to strong long-period motions from great earthquakes mentioned above.

We hope the basic theory and methodology described in this textbook are useful for graduate-course students and young researchers and engineer to understand for strong motion seismology.

Our work has been made with the supports given to our research projects over years, the Grants-in-Aid for Scientific Research and Special Project for Earthquake Disaster Mitigation in Urban Areas from Ministry of Education, Culture, Sports, Science and Technology of Japan, and Special Coordination Funds for Promoting Science and Technology Japan Science and Technology Agency. We would like to thank these organizations.

References

Irikura, K. and K. (2006). Predicting strong ground motions with “recipe”, *Bull. Earthq. Res. Inst. Univ. Tokyo*, **81**, 341-352

Irikura K. and S. Kurahashi (2008), New developments of strong motion prediction learning from recent disastrous earthquakes, *Fifth International Conference on Urban Earthquake Engineering, Tokyo Institute of Technology*, 15-24.

Kamae, K. and H. Kawabe (2008), Source Modeling and Strong Ground Motion Simulation the

2007 Niigata-ken Chuetsu-oki Earthquake (Mj 6.8) in Japan, *14th world conference of Earthquake Engineering, Beijing, China*.

Kawabe, H., K. Kamae, and K. Irikura (2008), Damage prediction of long-period structures during subduction earthquakes – Part 1: Long-period ground motion prediction in the Osaka basin for future Nankai earthquakes -, *14th world conference of Earthquake Engineering, Beijing, China*.

Nakagawa, Y., K. Kamae, H. Kawabe, and K. Irikura (2008), Damage prediction of long-period structures during subduction earthquakes – Part 1: Prediction of damage of high-rise buildings in the Osaka basin for future Nankai earthquakes -, *14th world conference of Earthquake Engineering, Beijing, China*.

Kojiro Irikura

Chapter 1: Predicting Strong Ground Motions with “Recipe”

地 震 研 究 所 彙 報
Bull. Earthq. Res. Inst.
Univ. Tokyo
Vol. 81 (2006) pp. 341–352

Predicting Strong Ground Motions with a "Recipe"

Kojiro Irikura[1),2)]*

[1)] Kyoto University
[2)] Aichi Institute of Technology

Abstract

A recipe is proposed for estimating strong ground motions from specific earthquakes based on source characteristics from waveform inversion using strong motion data. The main features of the source model are characterized by three kinds of fault parameters, which we call: outer, inner, and extra fault parameters. The outer fault parameters provide overall pictures of the target earthquakes such as entire source area and seismic moment. The inner fault parameters characterize stress heterogeneity inside the fault area. The extra fault parameters are considered to complete the source model, and include starting point and propagation pattern of the rupture. The seismic hazard maps for future large earthquakes with a high probability of occurrence potential are based on the idea of the recipe proposed here by two governmental organizations, the Headquarters of Earthquake Research Center and Central Disaster Prevention Council in Japan.

Key words: strong ground motion, outer fault parameter, inner fault parameter, asperity, effective stress

1. Introduction

From recent developments in waveform inversion analyses for estimating the rupture process using strong motion data during large earthquakes, we have understood that strong ground motions are related to slip heterogeneity inside the source rather than average slip in the entire rupture area. Asperities are characterized as regions that have a large slip relative to the average slip on the rupture area, based on heterogeneous slip distributions that are estimated from source inversion (Somerville *et al.,* 1999). It was found that the asperity areas, as well as entire rupture areas, scale with total seismic moment. Another important study for strong motion prediction showed that strong motion generation areas coincide approximately with asperity areas, where a lot of stress is released (Miyake *et al.,* 2001; Miyake *et al.,* 2003).

Based on the two scaling relationships for the entire rupture area and the asperity areas with respect to the total seismic moment, we found that the source model for predicting strong ground motions is characterized by three kinds of fault parameters: outer, inner, and extra fault parameters. The outer fault parameters are conventional parameters characterizing earthquake size, such as rupture area and seismic moment, and give an overall picture of a source fault. The inner fault parameters are introduced in this study as the combined area of asperities and stress drop of each asperity that define slip heterogeneity inside the source, and which have much more influence on strong ground motions. The extra fault parameters characterize rupture nucleation and termination such as starting point and propagation pattern of the rupture.

So far, most strong motion predictions in earthquake hazard analyses have been made using the empirical attenuation-distance curve for peak ground acceleration (PGA) and peak ground velocity (PGV), in which source information is defined only by seismic magnitude and fault area as outer fault parameters. However, from the source inversion studies mentioned above, we have realized that such parameters are not sufficient to estimate strong ground motions.

We developed a "recipe" for predicting strong

* e-mail: irikura@geor.or.jp (1–8–4, Utsubo-honmachi, Nishi-ku, Osaka, 550–0004, Japan)

ground motions (Irikura and Miyake, 2001; Irikura, 2004), which characterizes the three kinds of fault parameters of source modeling for future large earthquakes. The idea of the "recipe" has been applied in the Seismic Hazard Map for Specified Seismic Source Faults by the Headquarters for Earthquake Research Promotion and the Central Disaster Prevention Council in Japan.

2. Strong Motion Prediction Program in Japan

The basic policy for defining seismic hazard in Japan is based on the 1999 fundamental mission statement governing earthquake research over the next ten years as "The promotion of earthquake research—comprehensive basic policies for the promotion of seismic research through the observation, measurement, and survey of earthquakes," established by the Headquarters for Earthquake Research Promotion (Director: Ministry of Education, Culture, Sports, Science, and Technology). It initiated the creation of seismic hazard maps by promoting surveys of active faults, long-term evaluations of occurrence potential, and predictions of strong ground motions.

Two subcommittees were established under the Headquarters. One is Subcommittee for Long-term Evaluations, which was launched in 1995 to evaluate the probability of earthquake occurrence at active faults and plate boundaries. The other is Subcommittee for Strong Motion Evaluations, which was launched in 1998 to make seismic hazard maps using two different approaches—probabilistic and deterministic.

The probabilistic seismic hazard map is shown as the predicted likelihood of a ground motion level such as PGA, PGV, and seismic intensity occurring in a given area within a set time as shown in Fig. 1. It provides important information for land planning, design standards for structures, and educating people on seismic risks.

The deterministic seismic hazard map is shown as a distribution of ground motion levels predicted for individual specific earthquakes from assumed fault models. The strong ground motions at specific sites near each source fault are estimated as time history, based on the recipe characterizing the source and numerical synthesis of waveforms with a hybrid scheme. Long-period motions are calculated by the

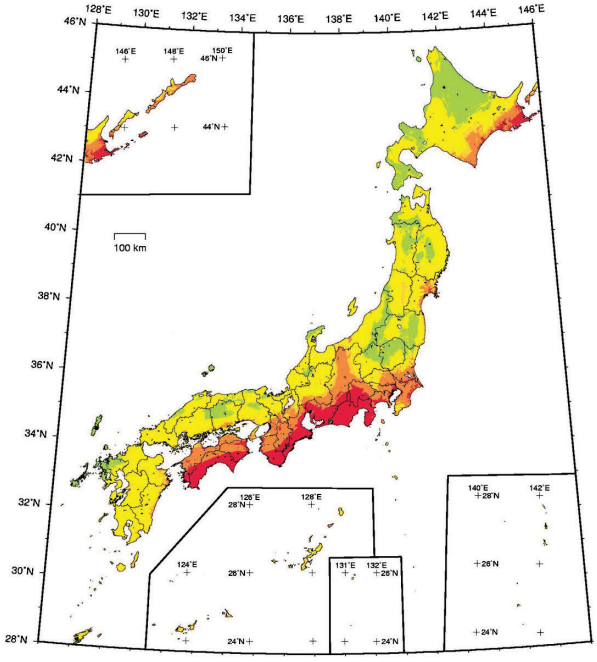

Fig. 1. Probability of suffering strong motions greater than seismic intensity 6- within 30 years from 2005 AD (Earthquake Research Committee, 2005).

finite difference method considering the 3-D structures from source to target sites, and short-period motions are simulated with the stochastic Green's function method (e.g. Irikura and Kamae, 1999). PGA, PGV, seismic intensity, etc., are easily evaluated once the time histories of ground motions are estimated. The time histories of ground motions are useful for nonlinear dynamic analyses of structures, which are needed to design earthquake-resistant buildings and critical structures such as bridges, lifelines, and electric power plants.

The Central Disaster Prevention Council belonging to the Cabinet Office also made deterministic seismic hazard maps for the hypothetical Tokai, Tonankai, and Nankai earthquakes shown as Fig. 2, which are feared likely to occur within the next half century. They made damage and causality estimates to determine disaster management plans for those earthquakes.

3. Scaling Relationships of Fault Parameters

Most of the difficulties predicting strong ground motions involve characterizing source models of future earthquakes. Conventional scaling relations of fault parameters such as fault length and average

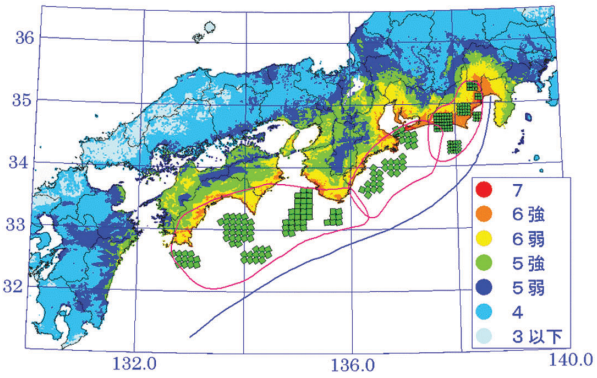

Fig. 2. Seismic intensity map from three hypothetical earthquakes, Tokai, Tonankai, and Nankai earthquakes continuously generated (Central Disaster Prevention Council, 2003).

slip on fault with seismic magnitude are mostly determined geologically from surface offsets and geophysically from forward source modeling using teleseismic data and geodetic data (e.g. Kanamori and Anderson, 1975). Such data are only available for very long period motions, but are not sufficiently available for near-source strong motions dominating short period motions of less than 1 sec of engineering interest. The scaling of fault parameters based on waveform inversion results of the source process using strong motion data gives a clue to solving this problem. We found two scaling relationships—one for the outer fault parameters and the other for the inner fault parameters.

Outer Fault Parameters

The scaling for the outer fault parameters, i.e., relationship between seismic moment and rupture area, for inland crustal earthquakes is summarized in Fig. 3 (a) (Irikura, 2004). For earthquakes with a relatively small seismic moment of less than 10^{19} Nm, the total fault area S seems to follow the self-similar scaling relation with a constant static stress drop in proportion to the two-thirds power of seismic moment M_0. The relation between M_0 and S is given by Eshelby (1957) assuming a circular crack with an average stress drop $\Delta\bar{\sigma}_c$.

$$M_0=\frac{16}{7\pi^{3/2}}\cdot\Delta\bar{\sigma}_c\cdot S^{3/2} \qquad (1)$$

For large earthquakes of more than 10^{19} Nm, scaling tends to depart from the self-similar model (Irikura and Miyake, 2001) corresponding to the saturation of fault width due to seismogenic zone size. Such a two-stage scaling relationship has also been found by Hanks and Bakun (2002). We add one more stage for extra-large earthquakes of more than 10^{21} Nm from the idea of Scholtz (2002), changing L-model to W-model. The scaling relationships in this study shown by broken lines in Fig. 3 (a) assume fault width saturates at a length of 20 km. The relation between M_0 and S for a larger aspect ratio of fault length L of width W is given by Fujii and Matsuura (2000), considering tectonic loading stress.

$$M_0=\frac{\Delta\bar{\sigma}_c W L^2}{aL+b} \qquad (2)$$

For the above equation, a and b are given at 1.4×10^{-2} and 1.0 by Fujii and Matsuura (2000).

Three-stage scaling also seems to be applicable for subduction earthquakes as shown in Fig. 3(b), although the bending points are different. Saturation of fault width for subduction earthquakes becomes longer.

Inner Fault Parameters

Strong ground motions are influenced by inner fault parameters representing slip heterogeneity more than outer fault parameters. The relationships between rupture area S, as the outer fault parameter, and combined area of asperities S_a, as the inner fault parameter, are shown in Fig. 4 (Irikura, 2004). The ratio S_a/S seems to be almost constant regardless of rupture area —about 0.22 for inland earthquake and about 0.25 for subduction earthquake. Then, stress drop on the asperities $\Delta\sigma_a$ is derived as a product of the average stress drop over the fault $\Delta\bar{\sigma}_c$ and the ratio of asperity area S_a to total rupture area S (e.g., Madariaga, 1979).

$$\Delta\sigma_a=\Delta\bar{\sigma}_c\cdot\frac{S}{S_a} \qquad (3)$$

Another empirical relationship between seismic moment M_0 and flat level of acceleration source spectrum A_0 related to inner source parameters is shown in Fig. 5; it was originally found by Dan *et al.* (2001),

$$A_0(dyne\cdot cm/s^2)=2.46\cdot10^{17}\cdot M_0^{1/3}, \qquad (4)$$

where the unit of M_0 is *dyne* · *cm*.

This relation was qualitatively confirmed by other authors (Morikawa and Fujiwara, 2003; Satoh, 2004), although the factor is different depending on

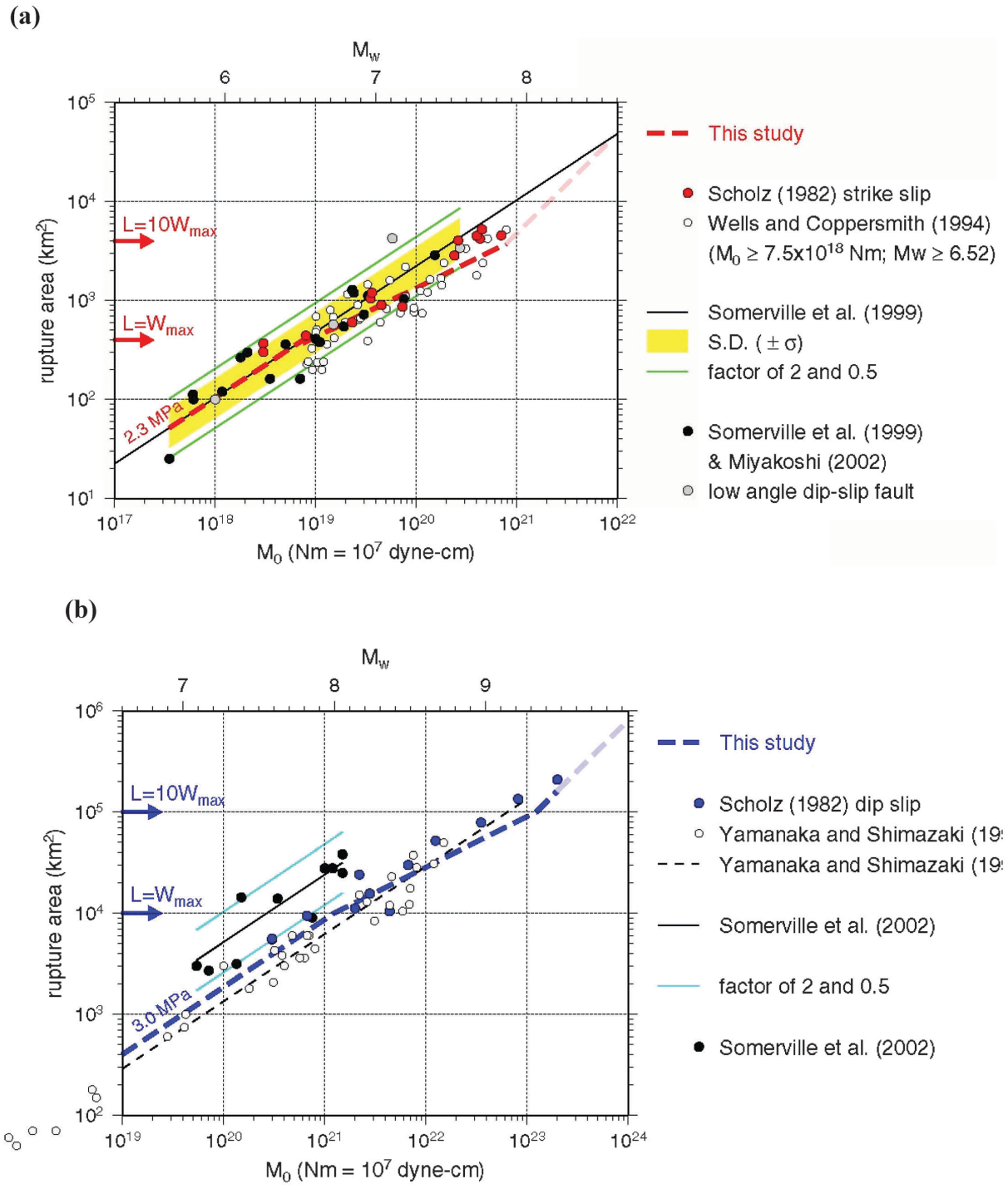

Fig. 3. Empirical relationships between seismic moment and rupture area for inland crustal earthquakes (a) and subduction earthquakes (b). Thick broken lines are 3-stage scaling relationships proposed by our studies (e.g. Irikura, 2004).

earthquake types such as inland-crustal, intra-slab, subduction (interplate) and regionality.

The acceleration source spectral level A_o is obtained by removing propagation-path and surface-geology effects from observed records. A_o is defined as

$$A_0=\sqrt{(A_0^a)^2+(A_0^b)^2},$$

where A_0^a is the acceleration spectral level from asperities and A_0^b is that from background areas.

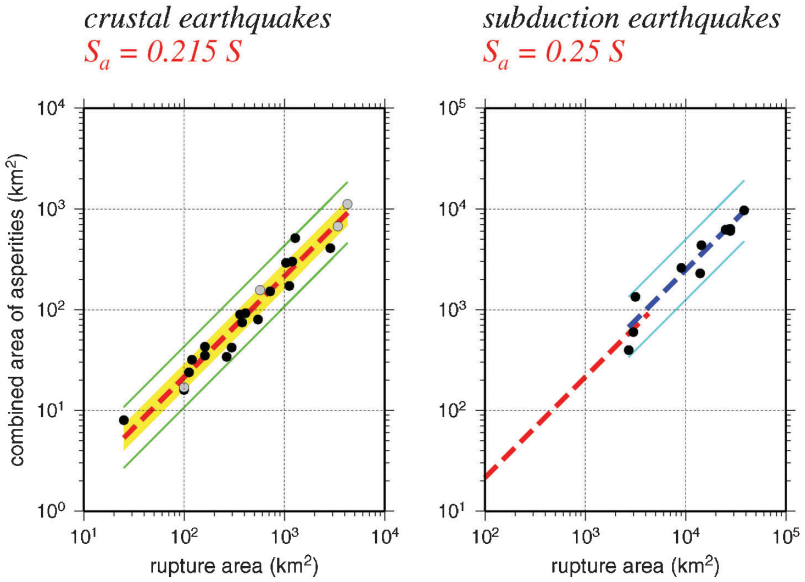

Fig. 4. Empirical relationships between combined area of asperities and total rupture area (thick broken line) for inland crustal earthquakes (left: after Irikura and Miyake, 2001) and subduction earthquakes (right). Shadow ranges $\pm\sigma$ (standard deviation). Thin solid lines show a factor of 2 and 1/2 for the average. Database obtained by the waveform inversions for the inland crustal earthquakes is Somerville *et al.* (1999) and Miyakoshi (2002), for the subduction earthquakes Somerville *et al.* (2002).

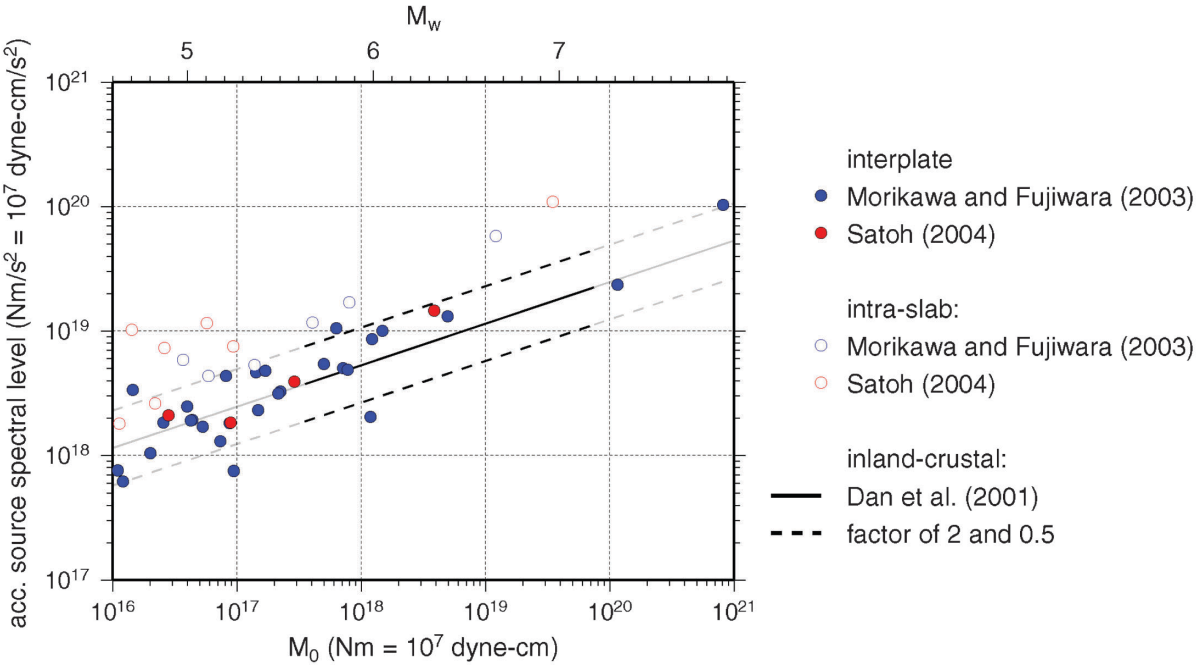

Fig. 5. Empirical relationship between seismic moment and acceleration source spectral level for inland crustal (solid line), intra-slab (open circle) and for subduction (interplate: solid circle) earthquakes.

The acceleration level A_0^a is theoretically proportional to the square root of the combined areas of asperities S_a and the stress drop in the asperities $\Delta\sigma_a$ by Madariaga (1977).

$$A_0^a = 4\sqrt{\pi}\,\beta v_r \Delta\sigma_a \sqrt{S_a}, \tag{5}$$

where β and v_r are S wave velocity of the media and rupture velocity. If A_0^b is relatively small compared to

A_0^a, A_0^a in (5) is replaced by A_0. Then, S_a is estimated as follows.

$$S_a=\left(\frac{7\pi^2}{4}\beta v_r\right)^2 \cdot \frac{(M_0)^2}{S \cdot (A_0)^2} \quad (6)$$

In this case the stress drop of the asperities $\Delta\sigma_a$ is also given as a product of $\Delta\bar{\sigma}_c$ and S/S_a using (3).

4. Recipe for Source Modeling

The procedure for characterizing the source model is outlined as a recipe for estimating three source parameters—outer, inner, and extra fault parameters—as follows:

Estimation of Outer Fault Parameters

Step 1: Total Rupture Area ($S=LW$)

Total fault length L of the specific earthquake is defined as the sum of the lengths of the fault segments grouping simultaneously activated. Fault width W is related to the total fault length before reaching the thickness of the seismogenic zone H_s, and is clipped at $H_s/sin\,\theta$ (θ: dip angle) after reaching there.

$$\begin{aligned} W(\mathrm{km}) &= L \ (\mathrm{km}) && \text{for } L < H_s/sin\theta \\ W(\mathrm{km}) &= H_s/sin\theta \ (\mathrm{km}) && \text{for } L >= H_s/sin\theta \end{aligned} \quad (7)$$

W seems to be clipped at about 20 km when θ is a low angle.

Step 2: Total Seismic Moment (M_0)

The total seismic moment is estimated from the relationship between seismic moment and rupture area (Fig. 3 (a) and (b)).

Step 3: Average Stress Drop ($\Delta\bar{\sigma}_c$) on the Fault

The average static stress-drop for rupture area at the first stage of Fig. 3 ($Mo<10^{19}$ Nm) is estimated by (1) for the circular crack model by Eshelby (1957).

Then, the average stress drop at the second and third stages of Fig. 3 is estimated by (2) for a larger aspect ratio by Fujii and Matsu'ura (2000).

Estimation of Inner Fault Parameters

Step 4. Combined Area of Asperities (S_a)

Two methods are used for the combined area of asperities S_a. One is taken from the empirical relation of S_a versus S (Somerville *et al.* 1999; Irikura and Miyake 2001), where the combined area of asperities is specified to be about 22%. The other is taken from (6), estimating the acceleration source spectral level either from the empirical relation such as (4) or observed records.

Step 5. Stress Drop on Asperities ($\Delta\sigma_a$)

As shown in (3), $\Delta\sigma_a$ as the inner fault parameter is derived as a product of $\Delta\bar{\sigma}_c$ as the outer fault parameter and S_a/S from Step 4.

Step 6. Number of Asperities (N)

The asperities in the entire fault rupture are related to the segmentation of the active faults. Locations of asperities are assumed from various information such as surface offsets measured along faults, back-slip rate studied by GPS observations, and weak reflection coefficients in fault planes.

Step 7: Average Slip on Asperities (D_a)

D_a is given as $2.0 \cdot D$ based on the empirical relationship of Somerville *et al.* (1999). This relationship is approximately confirmed from dynamic simulations of slip distribution with the multiple-asperity source model (Dalguer *et al,* 2004). More precisely, their results show that $D_a/D=2.3$ for $N=1$, $D_a/D=2.0$ for $N=2$, $D_a/D=1.8$ for $N=3$ (N: number of aerities) under constraint Sa/S=0.22 and stress drop of background area $\Delta\sigma_b=0.0$.

Step 8: Effective Stress on Asperity (σ_a) and Background Slip Areas (σ_b)

Effective stress σ_a on asperity for strong motion generation is considered to be identical to stress drop on asperity $\Delta\sigma_a$. Effective stress σ_b on background slip area is constrained by the empirical relationship between seismic moment and acceleration source spectral level.

Step 9: Parameterization of Slip-Velocity Time Functions

The Kostrov-like slip-velocity time functions are assumed as a function of peak slip-velocity and rise time, based on the results of the dynamic simulation of Day (1982). The peak slip-velocity is given as a function of effective stress, rupture velocity, and f_{max}.

Estimation of Extra Fault Parameters

The extra fault parameters are rupture starting point and rupture velocity, which characterize the rupture propagating pattern in the fault plane. For inland crustal earthquakes, rupture nucleation and termination are related to the geomorphology of active faults (e.g., Nakata *et al.*,1998; Kame and Yamashita, 2003). For subduction earthquakes, information from past earthquakes is applied as much as possible.

5. Applicability and Validity of "Recipe"

The "recipe" proposed here has been applied to deterministic seismic-hazard maps for specified seismic source faults with a high probability of occurrence potential in the National Seismic Hazard Maps for Japan (2005). The distribution of ground shaking levels such as PGV and seismic intensity has been evaluated for 10 inland crustal earthquakes and two subduction earthquakes. The availability of the "recipe" has been tested in each application by comparing PGV's of synthesized motions and those derived from the empirical attenuation relationship by Si and Midorikawa (1999).

A more detailed examination has been attempted to show the validity and applicability of the "recipe" comparing simulated ground motions with observed ones for inland crustal earthquakes and subduction earthquakes. We introduce two cases, one is the 1995 Kobe earthquake, as an example of the inland earthquake, and the other is the 2003 Tokachi-oki earthquake, as an example of the subduction earthquake.

1995 Kobe earthquake (Mw 6.9)

The source slip model of the 1995 Kobe earthquake was determined from the inversion of strong ground motion records by several authors (e.g. Sekiguchi *et al.,* 2000 and Yoshida *et al.,* 1996). The slip distributions on the fault plane are similar to each other, although there are clear differences depending on the frequency ranges of the data, smoothing techniques used, etc. Even if the inverted source model is almost uniquely determined, it is not always available for a strong motion simulation. The inversion is usually done using only long-period motions of more than 1 sec.; therefore, it might not be useful for broadband motions including short-period motions of less than 1 sec. of engineering interest.

Then, we refer to the slip model available for broadband ground motions derived from forward modeling using the empirical Green's function method (Kamae and Irikura, 1998). The model consists of three segments: two are at the Kobe side and one is at the Awaji side, as shown in Fig. 6 (a). The outer parameters are given, because the entire rupture area is 51×20.8 km^2, and the total seismic moment is 3.29×10^{23} MPa, assuming $\Delta\bar{\sigma}_c$ to be 2.3 MPa following Steps 1, 2, and 3. Next, the inner fault parameters are given as Sa/S is 0.22, then $\Delta\sigma_a$ is 10.5 MPa. One asperity is distributed in every segment (total of three asperities over the rupture area). The stress drop of the background area is estimated to be about 4.0 MPa from the difference between the stress drop of the asperity directly from Sa/S using (3) and that indirectly from the acceleration level using (5) and (6). Several models are examined to verify the influence of background effective stress σ_b on synthetic motions. Background effective stress σ_b is given as 0.0 MPa for Model 1 and as 4.0 MPa for Model 4. The other parameters are given following Step 4 through Step 9 as summarized in Fig. 6 (b).

Strong ground motions are calculated using the stochastic Green's function method (Kamae *et al.,* 1998). According to this method, the Green's functions are stochastically calculated based on band-limited-white-noise with spectra following the ω^{-2} model, and site effects empirically estimated from observed records of small events. The stochastic Green's functions are changeable depending on the random function in each trial. We choose one representation of those Green's functions whose spectra follow the omega-square model as faithfully as possible.

The synthesized acceleration and velocity motions for Models 1 and 4 are compared with observed motions at KBU very close to the source fault in Fig. 6 (c). The velocity motions show a very good fit between synthesized and observed ones at the right side of Fig. 6 (c), both of which have two significant directivity pulses on two asperities in the forward rupture direction. We find that the most important parameters featuring strong ground motions are sizes of asperities and effective stress on each asperity, which characterizes amplitudes and periods of directivity pulses causing earthquake damage. On the other hand, the synthesized acceleration motions have a larger peak than observed ones at the left side of Fig. 6 (c). There are two possibilities for overestimating acceleration motions. One is that uniform rupture velocity might cause too strong the directivity effect from an asperity near KBU to the synthesized acceleration motions. The other is due to the non-linear behavior of soil layers near the surface. Such high-frequency motions are less effective for evaluating instrumental seismic intensity.

Variability of the synthesized pseudo-velocity response spectra calculated from 10 trials with sto-

(a)

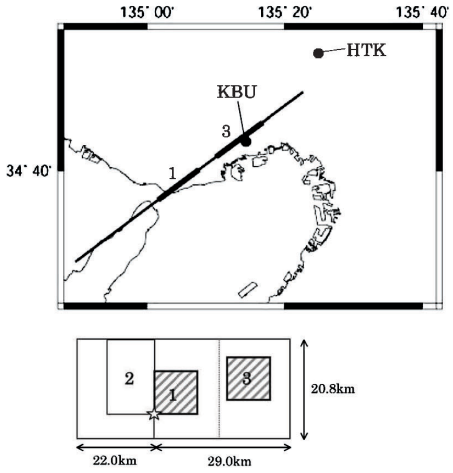

(b)

		M_0 dyne-cm	S km²	D cm	$\Delta\sigma$ MPa	A dyne-cm/sec²
total fault area		3.29×10^{26}	1062	103	2.3	1.70×10^{26}
segment 1	(total)	8.43×10^{25}	300	94	2.3	9.03×10^{25}
	(asperity)	3.57×10^{25}	64	186	10.5	7.29×10^{25}
	(background)	4.86×10^{25}	236	69	4.0	5.33×10^{25}
segment 2	(total)	1.60×10^{26}	462	115	2.3	1.12×10^{26}
	(asperity)	6.96×10^{25}	100	232	10.5	9.12×10^{25}
	(background)	9.04×10^{25}	362	83	4.0	6.50×10^{25}
segment 3	(total)	8.43×10^{25}	300	94	2.3	9.03×10^{25}
	(asperity)	3.57×10^{25}	64	186	10.5	7.29×10^{25}
	(background)	4.86×10^{25}	236	69	4.0	5.33×10^{25}

(c)

(d)

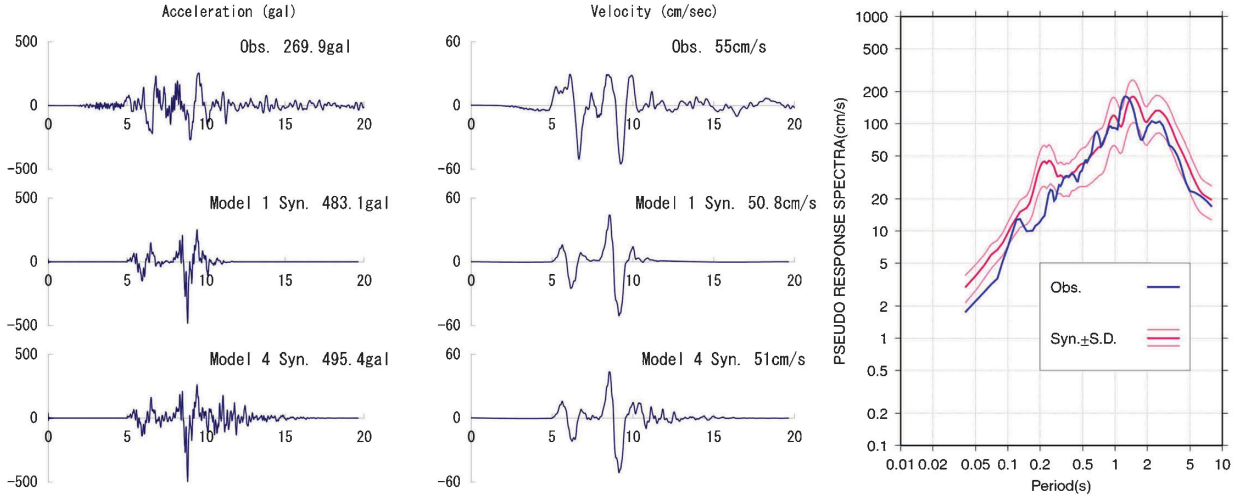

Fig. 6. Ground motion simulation of the 1995 Kobe earthquake using the stochastic Green's function method. (a) Characterized source model based on Kamae and Irikura (1998). (b) Source parameters for synthetic motions. (c) Comparison between observed and synthetic velocities of NS component at KBU station. (d) Variability of synthetic pseudo-velocity response spectra using 10 trials of stochastic Green's functions.

chastic Greens functions is shown for observed ones in Fig. 6 (d). The observed ones range within one standard deviation at periods longer than 0.2 sec, and are effective for measuring seismic intensity. Large deviations of synthesized motions at higher frequencies coincide with overestimation of acceleration motions. We find that strong ground motions from the Kobe earthquake using the "recipe" can be used in practice to predict distributions of seismic intensity.

2003 Tokachi-Oki Earthquake (Mw 8.0)

So far, very few strong motion records for subduction earthquakes have been obtained from around the world. Therefore, we only have less accurate inversion results from slip models of subduction earthquakes. The 2003 Tokachi-oki earthquake provided a large number of strong ground motion records including the source area. Slip models for the earthquake have been proposed by several authors using the waveform inversions of strong motion records (e.g. Honda *et al.*, 2004), teleseismic data (e.g. Yamanaka and Kikuchi, 2003), joint inversions of strong motion and teleseismic data (e.g. Yagi, 2004) and strong motion and geodetic data (Koketsu *et al.*, 2004), and so on.

These results gave us a great opportunity to discuss the validity and applicability of the recipe to subduction earthquakes.

Verification of estimating strong ground motions for this earthquake based on the "recipe" was shown in Report of the National Seismic Hazard Map (2005) by Earthquake Research Committee (2005). We outline the verification mentioned above. The location and geometry of the seismic source fault refer to Honda *et al.* (2004) as shown at the bottom right of Fig. 7. The rupture initiation point is taken at the epicenter determined by the Japan Meteorological Agency.

The order for setting the outer fault parameters is somewhat different from that of the inland earthquakes. The most stable and reliable parameter is seismic moment, which is adopted as $1.05\ 10^{21}$ N-m from the analysis of teleseismic data by Kikuchi and Yamanaka (2003). The rupture area is given to be 9000 km^2, assuming $\Delta\bar{\sigma}_c$ of 3.0 MPa (Kanamori and Anderson, 1975). That is, first *Mo,* second $\Delta\bar{\sigma}_c$ and third *S* are set in order.

The inner fault parameters are given as follows. First, the number of asperities is assumed to be three based on the source inversion results (Yamanaka and Kikuchi, 2003; Honda *et al.,* 2004; Koketsu *et al.,* 2004; Yagi, 2004). The locations of the three asperities are shown by the solid circles inside the source fault in Fig. 7, referring to the result obtained from the forward modeling using the empirical Green's function method of Kamae and Kawabe (2004). The area of the large asperity is 361.2 km^2, and that of the other two asperities is half of the large one. The stress drop of each asperity is estimated at 37.4 MPa from the empirical relation Mo vs acceleration level following Steps 4 and 5. The remaining parameters are given with the "recipe."

The synthesized motions are calculated using a hybrid method (Irikura and Kamae, 1999) with a crossover period of 5 sec, summing up longer period motions with a theoretical procedure and shorter period motions with the stochastic Green's function method. Examples are shown in Fig. 7, in which waveforms and pseudo-velocity-response spectra are compared between observed and synthesized motions at three sites, TKCH11, HDKH05, and HKD093 very near the source fault. We find that the synthesized motions agree well with the observe records.

The instrumental seismic intensity distributions estimated from the observed records and synthesized motions are shown at the left of Fig. 8. Comparison of the seismic intensity between observed records and synthesized motions is shown at the right of Fig. 8. The seismic intensities from the synthesized motions are generally consistent with the observed ones. However, we can see overestimated synthesized motions in some regions where thick sedimentary layers are underlying. This might be due to the empirical formula for estimating instrumental seismic intensity from peak ground velocity. This formula tends to overestimate instrumental seismic intensity with respect to ground motions having a predominant longer than 2 sec.

There still remain many other problems to solve in applying the "recipe" to the subduction earthquake. One of difficulties is to specify the number and locations of asperities when no historical records exist. The other problems arise from difficulties related to a lack of deep basin and off-shore structures from source areas to objective regions, detailed geometries of plate boundaries, etc.

6. Conclusions

A "recipe" for predicting strong ground motions for future large earthquakes is constructed from recent findings of earthquake source physics in seismology and structure damage mechanisms in earthquake engineering. Two scaling relationships are found from the results of the source process by waveform inversion using strong motion data: one is seismic moment M_o versus entire source area S for the outer fault parameters, and the other is M_o versus asperity areas S_a for the inner fault parameters.

The source model is defined by three kinds of fault parameters: outer, inner, and extra fault parameters following the "recipe" based on the scaling relationships. In this study the validity and applicability of the procedures for characterizing earthquake sources based on the "recipe" are examined in comparison with observed records and broad-band simulated motions for the 1995 Kobe and the 2003 Tokachi-oki earthquakes.

The synthesized ground motions following the "recipe" for the 1995 Kobe earthquake are consistent with observed records of velocity and seismic intensity, but overestimate acceleration at a very near

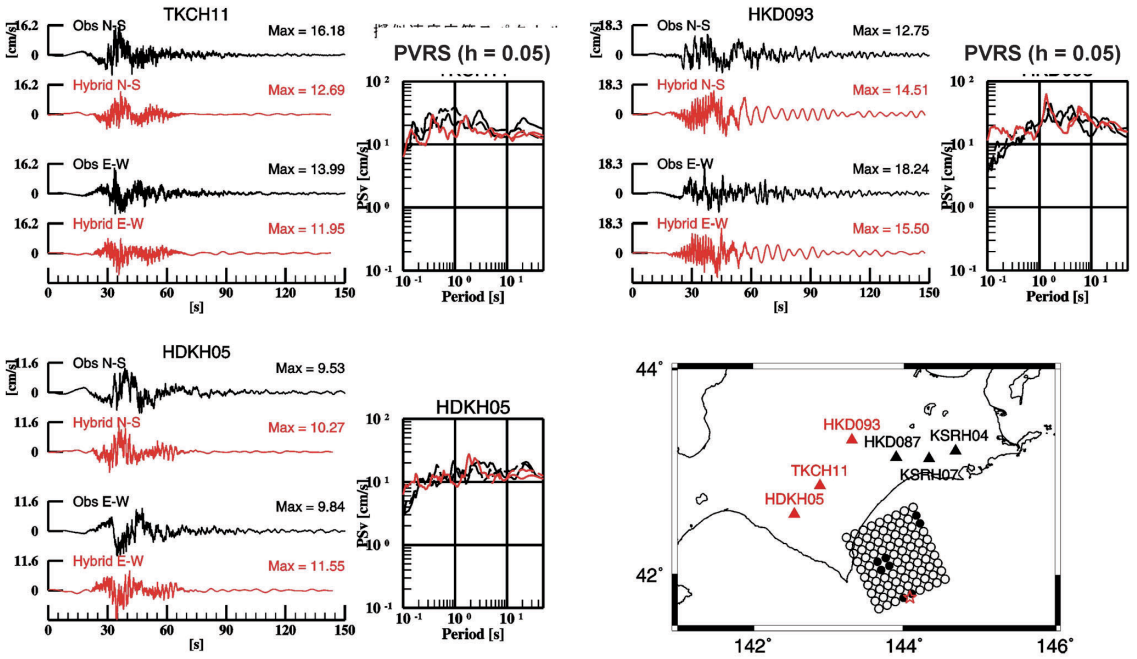

Fig. 7. Comparison of waveforms and pseudo-velocity-response spectra (PVRS, h=0.05) between those observed and synthesized from the 2003 Tokachi-oki earthquake. Map showing source model and observation stations is at the right bottom.

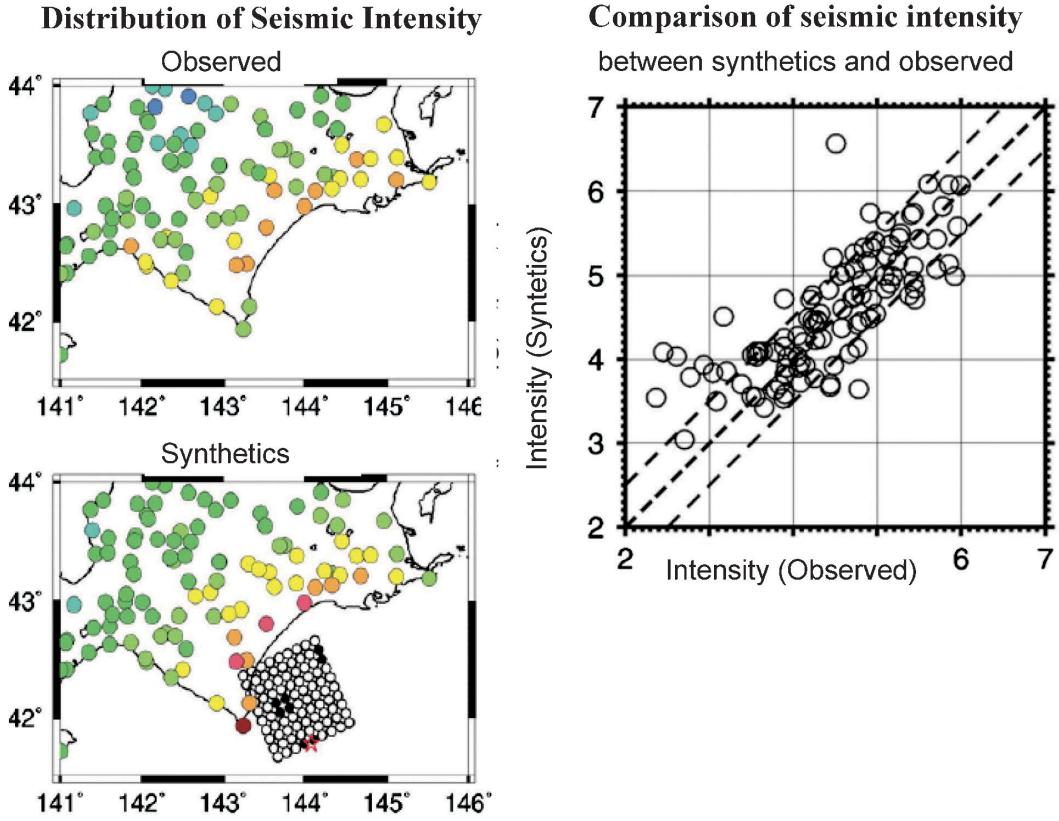

Fig. 8. Comparison of seismic intensity between observed and synthetics for the 2003 Tokachi-oki earthquake. Left: distribution of seismic-intensity from observed records (Upper map) and synthetic motions (Lower map). Left lower: comparison of seismic intensity between synthetics and observed.

station. The most important parameters featuring strong ground motions are sizes of asperities and effective stress on each asperity, which characterize the amplitudes and periods of directivity pulses causing earthquake damage.

The ground motions for the 2003 Tokachi-oki earthquake, as an example of a subduction earthquake, are successfully simulated based on the "recipe," showing good agreement in the spatial pattern of seismic intensity, as well as in the waveform between observed and synthetics. However, we need a priori information for specifying the number of asperities and their locations, as well as the location and geometry of the source fault. It is very difficult to specify such source parameters when no historical records exist.

Acknowledgments

This study was done as a part of the governmental project of "National Seismic Hazard Map in Japan" sponsored by the Headquarters for Earthquake Research Promotion of Japan under the Ministry of Education, Culture, Sports, Science, and Technology. I express deep thanks for allowing me to refer to the results and figures of the Seismic Hazard Map presented by the Earthquake Research Committee. I am grateful to Hiroe Miyake and Katsuhiro Kamae for their contributions to this study.

References

Central Disaster Prevention Research Institute, 2003, Estimated Seismic Intensity Distribution in the case of Simultaneous Occurrence of Three Earthquakes, Tokai, Tonankai, and Nankai, 16th Special Survey Committee of Tonankai and Nankai earthquake, http://www.bousai.go.jp/jishin /chubou/nankai/16/index.html (in Japanese).

Dalguer, L.A., H. Miyake, K. Irikura, 2004, Characterization of dynamic asperity source models for simulating strong ground motions, *Proceedings of the 13th World Conference on Earthquake Engineering,* No.3286, CD-ROM.

Dan K, Watanabe T, Sato T, Ishii T., 2001, Short-period source spectra inferred from variable-slip rupture models and modeling of earthquake fault for strong motion prediction, *Journal of Struct. Constr. Engng. AIJ,* **545**, 51–62.

Das S and B.V. Kostrov, 1986, Fracture of a single asperity on a finite fault, *Earthquake Source Mechanics, Geophysical Monograph 37, Maurice Ewing Series* **6**, *American Geophysical Union,* 91–96.

Day, S.M., 1982, Three-dimensional simulation of spontaneous rupture: the effect of nonuniform prestress, *Bull. Seism. Soc. Am.,* **88**, 512–522.

Earthquake Research Committee, 2005, National Seismic Hazard Map for Japan (2005), *Report published by the Headquarters of Earthquake Research Promotion under the Ministry of Education, Culture, Sports, Science, and Technology,* 121p. (in Japanese).

Earthquake Research Committee, 2005, 4.3.13 Verification results using observed records of the 2003 Tokachi-Oki Earthquake, *National Seismic Hazard Map for Japan (2005),* http://www.jishin.go.jp/main/index-e.html

Eshelby J.D., 1957, The determination of the elastic field of an ellipsoidal inclusion, and related problems," *Proc.. Roy Soc.,* **A241**, 376–396.

Fujii, Y. and M. Matsu'ura, 2000, Regional difference in scaling laws for large earthquakes and its tectonic implication, *PAGEOPH,* **157**, 2283–2302.

Hanks, T.C. and W.H. Bakun, 2002, A bilinear source-scaling model for M-logA observations of continental earthquakes, *Bull. Seism. Soc. Am,* **92,** 1841–1846.

Honda, R., S. Aoi, N. Morikawa, H. Sekiguchi, K. Kunugi and H. Fujiwara, 2004, Ground motion and rupture process of the 2003 Tokachi-oki earthquake obtained from strong motion data of the K-NET and KiK-net, *Earth Planets and Space* **56**, 317–322.

Irikura K., 2004, Recipe for predicting strong ground motion from future large earthquake, *Annuals of Disaster Prevention Research Institute,* **47A**, 25–45 (in Japanese).

Irikura K and K. Kamae, 1999, Strong ground motions during the 1948 Fukui earthquake, *Zisin,* **52**, 129–150 (in Japanese).

Irikura K. and H. Miyake H., 2001, Prediction of strong ground motions for scenario earthquakes, *Journal of Geography,* **110**, 849–875 (in Japanese with English abstract).

Kame N. and T. Yamashita T., 2003, Dynamic branching, arresting of rupture and the seismic wave radiation in self-chosen crack path modeling, *Geophys. J. Int.,* **155**, 1042–1050.

Kamae K. and K. Irikura, 1998, Rupture process of the 1995 Hyogo-ken Nanbu earthquake and simulation of near-source ground motion, *Bull. Seism. Soc. Am.,* **88**, 400–412.

Kamae, K., K. Irikura and A. Pitarka, 1998, A technique for simulating strong ground motion using hybrid Green's function, *Bull. Seism. Soc. Am.,* 88, 357–367.

Kamae, K. and H. Kawabe, 2004, Source model composed of asperities for the 2003 Tokachi-oki, Japan, earthquake (M_{JMA}=8.0) estimated by the empirical Green's function method, *Earth Planets and Space* **56**, 323–327.

Kanamori H. and D.L. Anderson, 1975, Theoretical basis of some empirical relations in seismology, *Bull. Seism. Soc. Am.,* **86**, 1073–1095.

Kikuchi M. and Y. Yamanaka, 2001, Rupture processes of past large earthquakes=Identification of asperities, *Seismo,* **5**, 6–7.

Koketsu, K., K. Hikima, S. Miyazaki and S. Ide, 2004, Joint inversion of strong motion and geodetic data for the source rupture process of the 2003 Tokachi-oki, Hokkaido, earthquake, *Earth Planets and Space* **56**, 329–334.

Madariaga, R., 1977, High frequency radiation from crack (stress drop) models of earthquake faulting, *Geophys. J. R. Astron. Soc.,* **51**, 625–651.

Madariaga, R., 1979, On the relation between seismic moment and stress drop in the presence of stress and strength heterogeneity, *J. Geophys. Res.,* **84**, 2243–2250.

Miyake, H., T. Iwata and K. Irikura, 2001, Estimation of rupture propagation direction and strong motion generation area from azimuth and distance dependence of source amplitude spectra, *Geophys. Res. Lett.,* **28**, 2727–2730.

Miyake H, T. Iwata, K. Irikura, 2003, Source characterization for broadband ground motion simulation: Kinematic heterogeneous source model and strong motion generation area, *Bull. Seism. Soc. Am.,* **93**, 2531–2545.

Miyakoshi, K., T. Kagawa, H. Sekiguchi, T. Iwata and K. Irikura, 2000, Source characterization of inland earthquakes in Japan using source inversion results, *Proc. 12 th World Conf. Earthq. Eng.* (CD-ROM).

Morikawa N. and H. Fujiwara, 2003, Source and path characteristics for off Tokachi-Nemuro earthquakes, *Programme and Abstracts for the Seismological Society of Japan, 2003 Fall Meeting,* 104 (in Japanese).

Nakata T, Shimazaki K, Suzuki Y, Tsukuda E., 1998, Fault branching and directivity of rupture propagation, *Journal of Geography,* **107**, 512–528 (in Japanese).

Satoh T., 2004, Short-period spectral level of intraplate and interplate earthquakes occurring off Miyagi prefecture, *Journal of JAEE'2004,* **4**, 1–4 (in Japanese with English abstract).

Scholz, C.H., 1982, Scaling laws for large earthquakes: Consequences for physical models, *Bull. Seism. Soc. Am.,* **72**, 1–14.

Scholz C.H., 2002, The mechanics of earthquakes and faulting, *Cambridge University Press.*

Sekiguchi, H., Irikura, K. and Iwata, T., 2000, Fault geometry at the rupture termination of the 1995 Hyogo-ken Nanbu earthquake, *Bull. Seism. Soc. Am.,* **90**, 974–1002.

Si, H. and S. Midorikawa, 1999, New attenuation relationships for peak ground acceleration and velocity considering effects of fault type and site condition, *J. Struct. Constr. Eng., AIJ,* **523**, 63–70 (in Japanese with English abstract).

Somerville P, K. Irikura, R. Graves, S. Sawada, D. Wald, N. Abrahamson, Y. Iwasaki, T. Kagawa, N. Smith, A. Kowada, 1999, Characterizing earthquake slip models for the prediction of strong ground motion, *Seism. Res. Lett.,* **70**, 59–80.

Somerville, P.G., T. Sato, T. Ishii, N.F. Collins, K. Dan and H. Fujiwara, 2002, Characterizing heterogeneous slip models for large subduction earthquakes for strong ground motion prediction. *Proc. 11th Japan Earthquake Symposium.*

Wells, D.L. and K.J. Coppersmith (1994): New empirical relationships among magnitude, rupture length, rupture width, rupture area, and surface displacement, *Bull. Seism. Soc. Am.,* Vol. 84, pp. 974–1002.

Yagi, Y., 2004, Source rupture process of the 2003 Tokachi-oki earthquake determined by joint inversion of teleseismic body wave and strong ground motion data, *Earth Planets and Space* **56**, 311–316.

Yamanaka Y, M. Kikuchi M, 2003, Source process of the recurrent Tokachi-oki earthquake on September 26, 2003, inferred from teleseismic body waves, *Earth Planets Space,* **55**, e21–e24.

Yoshida, S., K. Koketsu, B. Shibazaki, T. Sagiya, T. Katoand Y. Yoshida, 1996, Joint inversion of the near- and far-field waveforms and geodetic data for the rupture process of the 1995 Kobe earthquake, *J. Phys. Earth,* **44**, 437–454, 1996.

(Received September 14, 2006)
(Accepted February 24, 2007)

Chapter 2: New Developments of Strong Ground Motion Prediction Learning from Recent Disastrous Earthquakes

NEW DEVELOPMENTS OF STRONG MOTION PREDICTION LEARNING FROM RECENT DISASTROUS EARTHQUAKES

Kojiro Irikura[1], and Susumu Kurahashi[2]

1) Adjunct Professor, Aichi Institute of Technology, Japan
2) PhD candidate, Aichi Institute of Technology
irikura@geor.or.jp, q05801@aitech.ac.jp

Abstract: Strong motion prediction has been progressed for promoting earthquake countermeasures learning from severe disasters of the 1995 Kobe earthquake. "National Seismic Hazard Map" has been made as one of national projects integrating all fields of earthquake researches such as active fault, earthquake forecast and strong motion prediction studies after the Kobe earthquake. Ground motions from earthquakes caused to specified source faults are evaluated based on "recipe". Verification and applicability have been examined by comparing observed ground motions with synthesized ones estimated using the "recipe". The 2007 Chuetsu-oki earthquake happened very close to the Kasiwazaki-Kariwa Nuclear Power Plant. The active faults caused to the earthquake have not been specified for the aseismic design of the plant. Ground motions from the earthquake are found to be predictable as long as the source fault is specified through investigation of active folds and faults. Further improvements of the fault modeling are required to make more reliable evaluation of ground motions for earthquake safety designs.

1. INTRODUCTION

Importance of strong motion prediction has been widely recognized for promoting earthquake-counter measures as one of the lessons of the 1995 Kobe earthquake, The Headquarter of Earthquake Research Promotion established just after the earthquake have developed "National Seismic Hazard Maps" (Earthquake Research Committee 2005). It should be more precisely called to be "Maps of Strong Motion Prediction in Japan". The maps show results of prediction of strong ground motions from two different approaches, probabilistic and deterministic, integrating survey of active faults, long-term evaluation for earthquake activities, and evaluation of strong ground motion. The probabilistic hazard maps show the probability of ground motion larger than seismic intensity 6-lower, occurring within 30 years from the present. On the other hand, the deterministic hazard maps show the levels of ground motions from earthquakes caused to specific active faults, based on fault models obtained from the active fault information.

The procedures of fault modeling for the prediction of strong ground motion are proposed as a recipe combining the active fault information with scaling relations of fault parameters from the waveform inversion of source processes using strong ground motions. This technique is introduced to the "Regulatory Guide for Aseismic Design of Nuclear Power Reactor Facilities" revised in 2006 by the Nuclear Safety Commission of Japan.

The 2007 Niigata-ken Chuetsu-oki happened very close to the Kasiwazaki-Kariwa Nuclear Power Plant that has the largest electric output in the world. It triggered a fire at an electrical transformer and other problems in the Plant. However, no problems have been confirmed with regard to the safety of the nuclear reactors as four of the plant's seven reactors running at the time of the earthquake were all shut down automatically by a safety mechanism according to the reports by the International Atomic Energy Agency (IAEA 2007) as well as the Nuclear and Industrial Safety Agency in Japan (NISA 2007).

There was recorded ground acceleration of 680 gals on the base mat of Unit No.1 reactor, 2.5 times more than the ground motion levels for aseismic design of facilities. The active faults caused to the earthquake have not been specified in evaluating input ground motions for the aseismic design. We need to make careful examinations why the active faults have been missed and how the ground motions have been underestimated.

In this report, we outline strong motion prediction for active faults, verification of recipe for strong motion prediction for recent disastrous earthquakes, e.g. simulations of the 2007 Chuetsu-oki earthquake and some other earthquakes, and prospect of strong motion prediction for promoting earthquake-counter measures, and overviews of strong motion predictions. Fifth International Conference on Urban Earthquake Engineering will be held on March 4-5, 2008 at Kokuyo Hall, Shinagawa-Ku, Tokyo, Japan. This document describes, and is formatted in, a required style of the conference paper.

2. OUTLINE OF STRONG MOTION PREDICTION

We have understood that strong ground motions are related to slip heterogeneity inside the source rather than average slip in the entire rupture area from recent studies of rupture process using strong motion data during large earthquakes. Asperities are characterized as regions that have a large slip relative to the average slip in the rupture area, based on heterogeneous slip distributions that are estimated from the waveform inversion (Somerville et al. 1999). We also found that strong motion generation areas coincide approximately with asperity areas, where a lot of stress is released (Miyake et al. 2001, Miyake et al. 2003). The asperity areas as well as the entire rupture areas scale with total seismic moments.

2.1 Scaling Relationships of Fault Parameters

One of the most important ideas for strong motion prediction is the scaling relationships of fault parameters. The conventional scaling relations of fault parameters such as rupture area and average slip on fault with seismic moment are mostly determined geologically from surface offsets and geophysically from forward source modeling using teleseismic data and geodetic data (e.g. Kanamori and Anderson 1975). Those fault parameters are only available for simulating very long period motions, but are not sufficiently available for near-source strong motions dominating short period motions of less than 1 sec of engineering interest.

We found new scaling relations of the asperity areas, as well as entire rupture areas, with respect to total seismic moment from the results of the waveform inversion mentioned above. Therefore, there are two kinds of the scaling relationships. One is the conventional scaling relations such as rupture area versus seismic moment and fault slip versus seismic moment. The other is the new ones such as asperity area versus seismic moment and asperity slip versus seismic moment. Based on the two kinds of scaling relationships for the entire rupture area and the asperity areas with respect to the total seismic moment, the source model for predicting strong ground motions is characterized by three parameters: outer, inner, and extra fault parameters.

The scaling for the outer fault parameters, i.e. relationship between seismic moment and rupture area, for inland crustal earthquakes are summarized as shown in Fig. 1 (Irikura 2004). For earthquakes with relatively small seismic moment less than 10^{19} Nm, the total fault area S seems to follow the self-similar scaling relation with constant static stress drop in proportion to the two-thirds power of seismic moment M0. For large earthquakes more than 10^{19} Nm, the scaling tends to depart from self-similar model (Irikura and Miyake 2001) corresponding to the saturation of fault width due to the seismogenic zone size. Further, one more stage should be added for extra large earthquakes more than 10^{21} Nm from the idea of Scholtz (2002) as changing from L-model into W-model. The scaling relationships in this study as shown by broken lines in Fig. 1 are drawn assuming the fault width saturates with 20 km long.

The inner fault parameters are introduced in this study as the combined area of asperities and stress drop of each asperity that define slip heterogeneity inside the source fault and that have much more influence on strong ground motions than the outer fault parameters. The relationships between rupture area S as the outer fault parameter and combined area of asperities S_a as the inner fault parameter are shown in Fig. 2 (Irikura 2004). The ratio S_a / S seems to be almost constant regardless of the rupture area, about 0.22 for the inland earthquake.

Then, stress drop on the asperities $\Delta\sigma_a$ is derived as a product of the average stress drop over the fault $\Delta\overline{\sigma}_c$ and the ratio of asperity area S_a to total rupture area S (e.g., Madariaga 1979).

$$\Delta\sigma_a = \Delta\overline{\sigma}_c \cdot S/S_a \tag{1}$$

Another empirical-relationship between seismic moment Mo and flat level of acceleration source spectrum A_o related to the inner source parameters is shown in Fig. 3, initially found by Dan et al. (2001) and confirmed by other authors (Morikawa and Fujiwara 2003, Satoh 2004).

$$A_0 = 2.46 \cdot 10^{17} \cdot (M_0 \cdot 10^7)^{1/3} \tag{2}$$

, where the unit of M_0 is $N \cdot m$.

The acceleration level A_0^a generated from the asperities is theoretically proportional to the square root of the combined areas of asperities S_a and the stress drop in the asperities $\Delta\sigma_a$ by Madariaga (1977). A_0^a is replaced by acceleration level from theoretical level A_0 from the total criteria because short-period motions mostly are mostly generated from the asperities.

$$A_0^a = 4\sqrt{\pi}\beta v_r \Delta\sigma_a \sqrt{S_a} \tag{3}$$

where β and v_r are S wave velocity of the media and rupture velocity.

Then, S_a is estimated as follows.

$$S_a = \left(\frac{7\pi^2}{4}\beta v_r\right)^2 \cdot \frac{(M_0)^2}{S \cdot (A_0)^2} \tag{4}$$

In this case the stress drop of the asperities $\Delta\sigma_a$ is also given as a product of $\Delta\overline{\sigma}_c$ and S/S_a using (1).

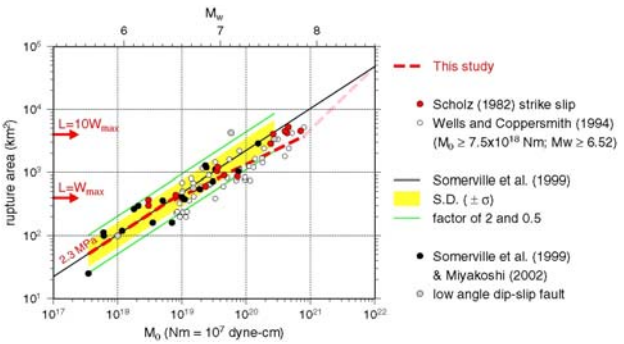

Figure 1 Empirical relationships between seismic moment and rupture area for inland crustal earthquakes (Irikura and Miyake, 2002).

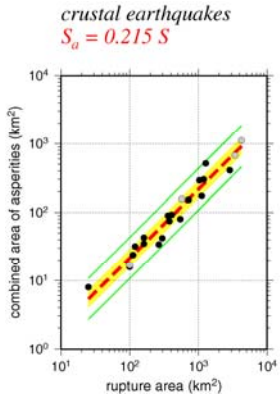

Figure 2 Empirical relationships between combined area of asperities and total rupture area (thick broken line) for inland crustal earthquakes (Irikura and Miyake, 2002). Shadow ranges (standard deviation). Thin solid lines show a factor of 2 and 1/2 for the average. Database obtained by the waveform inversions for the inland crustal earthquakes is Somerville et al. (1999) and Miyakoshi (2002)

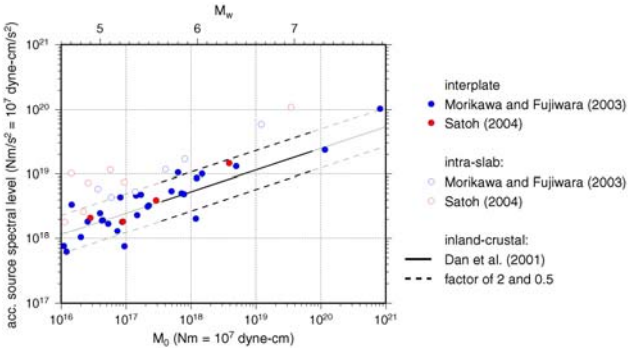

Figure 3 Empirical relationship between seismic moment and acceleration source spectral level for inland crustal earthquakes.

2.2 Recipe for Source Modeling

Strong motions for large earthquakes are simulated, based on characterized source models defined by three kinds of parameters, outer, inner, and extra fault parameters. We developed a "recipe" for predicting strong ground motions (Irikura and Miyake 2001, Irikura 2004) to characterize those fault parameters of source modeling for future large earthquakes.

The source model is constructed by the following procedure. First, the outer fault parameters are given as follows. Step 1: Total Rupture Area ($S = LW$) is given from investigations of active faults. Step 2: Total Seismic Moment (M_0) is given from the empirical scaling relation, M_0 versus S. Step 3: Average Stress Drop ($\Delta\overline{\sigma}_c$) on the source fault is estimated from the theoretical equation for circular crack model by Eshelby (1957) at the first stage of Fig. 1 (Mo < 10^{19} Nm) and another equation by Fujii and Matsu'ura (2000) at the second and third stages of Fig. 1.

Second, the inner fault parameters are given to characterize stress heterogeneity inside the fault area. Step 4: Combined Area of Asperities (S_a) is estimated from the acceleration source spectral level based on the empirical relation such as (2) or observed records. Step 5: Stress Drop on Asperities ($\Delta\sigma_a$) is derived as a product of $\Delta\overline{\sigma}_c$ as the outer fault parameter and S_a/S from Step 4. Step 6: Number of Asperities (N) is related to the segmentation of the active faults, e.g. two per a segment. Step 7: Average Slip on Asperities (D_a) given as $2.0 \cdot D$ based on the empirical relationship by Somerville et al. (1999). Step 8: Effective Stress on Asperity (σ_α) and Background Slip Areas (σ_β) is considered to be identical to stress drop on asperity $\Delta\sigma_\alpha$. Step 9: Parameterization of Slip-Velocity Time Functions is given to be the Kostrov-like slip-velocity time functions as a function of peak slip-velocity and rise time based on the results of dynamic simulation by Day (1982). The peak slip-velocity is given as a function of effective stress, rupture velocity and f_{max}.

The extra fault parameters are the rupture starting point and rupture velocity to characterize the rupture propagating pattern in the fault plane. For inland crustal earthquakes, rupture nucleation and termination are related to geomorphology of active faults (e.g., Nakata et al. 1998, Kame and Yamashita 2003).

3. APPLICABILITY OF STRONG MOTION PREDICTION RECIPE

Strong motions for large earthquakes are simulated, based on characterized source models defined by three kinds of parameters, outer, inner, and extra fault parameters. Those fault parameters are defined by the "recipe" of strong motion prediction. This "recipe" has been applying to deterministic seismic-hazard maps for specified seismic source faults with high probability of occurrence potential in the National Seismic Hazard Maps for Japan (2005). The availability of the "recipe" has been tested in each application by the comparison between PGV's of the synthesized motions and those derived from empirical attenuation relationship by Si and Midorikawa (1999). More detailed examination for strong motion prediction should be made, comparing simulated ground motions with observed ones for recent disastrous earthquakes.

3.1 Simulation of Ground Motions for the 2007 Niigata-ken Chubu Earthquake (Mw=6.6)

This earthquake occurred on July 16, 2007, northwest off Kashiwazaki in Niigata Prefecture, Japan, causing severe damage such as ten people dead, about 1300 injured, about 1000 collapsed houses and major lifelines suspended to near-source region. In particular, strong ground motions from the earthquake struck the Kashiwazaki-Kariwa nuclear power plant (hereafter KKNPP), triggering a fire at an electric transformer and other problems such as leakage of water containing radioactive materials into air and the sea, although the radioactivity levels of the releases are as low as those of the radiation of the natural environment in a year.

We attempt to simulate strong ground motions during the 2007 Chuetsu-oki earthquake based on the characterized source model. It is to examine the predictability of the ground motions with specified source model given by the "recipe".

The source mechanism of this earthquake is supposed to be a reverse fault with the SW-NE strike and SE dip from the aftershock distribution re-determined using the OBS seismometers (ERI, Univ. of Tokyo 2008) as shown in Fig. 4. Results of the rupture processes inverted by using strong motion data show the source fault with the SW-NE strike and SE dip gives slip distribution to match well observed data (Hikima and Koketsu 2007).

The PGA attenuation-distance relationships in Fig. 5 generally follow the empirical relations in Japan obtained by Si and Midorikawa (1999) except the KKNPP. The strong ground motions in the site of the KKNPP had markedly large accelerations more than those expected from the empirical relations. The surface motions there had the PGA of more than 1200 gals and even underground motions on one of the base-mats of the reactors locating five stories below the ground had the PGS of 680 gals. The PGA's recorded at underground rock sites of the KKNPP are significantly larger than those expected from the empirical relationship by Fukushima and Tanaka (1990).

The observed records close to the mainshock had two or three distinctive pulses, in particular, three significant pulses at stations on the base-mats of the Nuclear Reactors of the KKNPP site. We estimated the locations of asperities using time differences between those pulses. We found that three asperities are located south-west and south of the hypocenter in Fig. 6. In this study, we called those asperities to be ASP1, ASP2 and ASP3. We chose appropriate records of aftershocks as the empirical Green's function, taking into account locations and fault mechanisms of the aftershocks. As a result, we adopted the record of Aftershock 1 on July 16 at 21:08 for ASP 1 and ASP2, and Aftershock 2 on August 4 at 0:16 for ASP3. Table 1 shows the source information about the mainshock and aftershocks and Table 2 shows the parameters of the fault plane used in this study.

We obtained the best-fit model by forward modeling to minimize the residuals between the observed and synthesized. The areas of three asperities were about 30 km^2 and stress drop were 20 – 24 MPa that are summarized in Table 3. The synthesized motions at KKZ1R2, KKZ5R2, NIG005 and NIG018 are compared with the observed ones in Fig. 7. The synthesized waveforms agree with the observed ones fairly well. In particular, three pulses appearing in the observed records at KKZ1R2 and KKZ5R2 located at B5F in underground of Unit 1 and Unit 5, respectively, are well reproduced in the synthesized velocity and displacement.

Table 1 The information of the mainshock and aftershocks used as the empirical Green's function.

	Mainshock	Aftershock(AFT1)	Aftershock(AFT2)
Origin time	07/07/16 10:13	07/07/16 21:08	07/08/04 00:16
Hypocenter	37.557, 138.609	37.509, 138.630	37.420, 138.537
Depth	12km	15.6km	13.1km
Mw	6.6	4.4	-
Mo	8.37E+16Nm	5.21E+16Nm	1.56E+14Nm

Table 2 The fault plane of the mainshock. The strike and dip were used from aftershock distributions by ERI, Univ. of Tokyo.

strike	dip	rake	Latitude	Longitude	depth
30	40	90	37.343	138.392	6.2km

Table 3 Source parameters for each asperity.

	Rupture start point	Depth (km)	Mo (Nm)
ASP1	(4,3)	12.3	1.69×10^{18}
ASP2	(5,5)	11.0	1.69×10^{18}
ASP3	(4,7)	12.0	1.02×10^{18}
	L (km)× W (km)	$\Delta\sigma$ (MPa)	Risetime (second)
ASP1	5.5×5.5 (N:5×5)	23.7	0.5
ASP2	5.5×5.5 (N:5×5)	23.7	0.5
ASP3	5.04×5.04 (N:9×9)	19.8	0.45

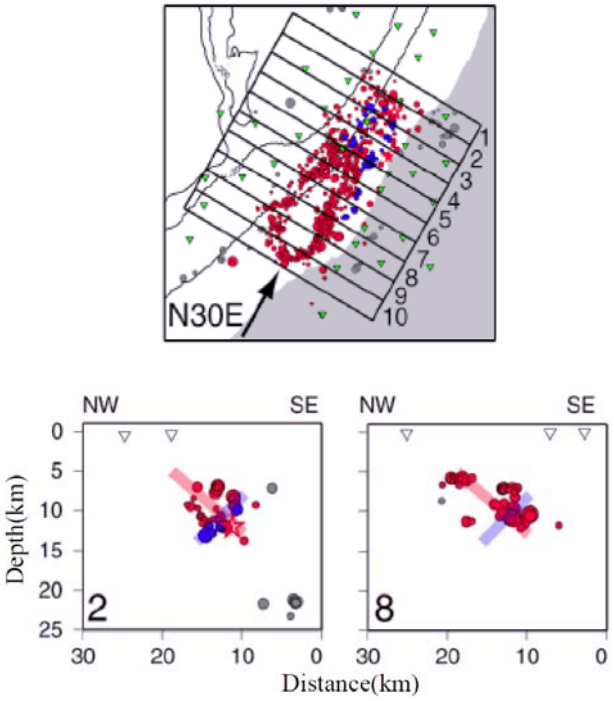

Figure 4 Aftershock distributions in the horizontal plane (upper) and cross section perpendicular to the strike (lower) using the OBS seismometers (ERI, Univ. of Tokyo,2008).

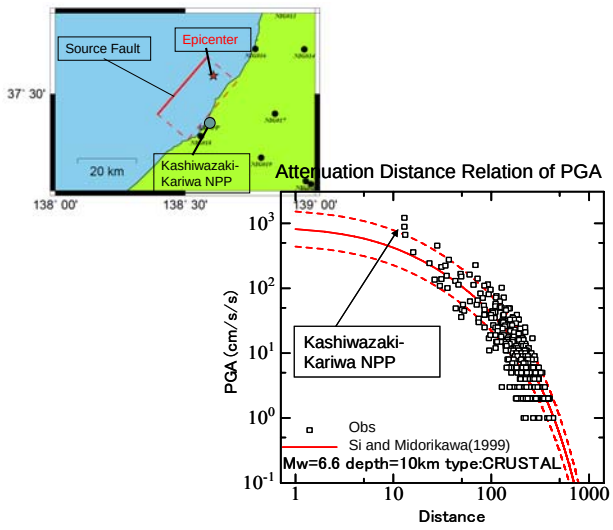

Figure 5 Upper: Map showing source fault by Horikawa (2007) and observation sites. Lower: Relationship of observed peak horizontal ground accelerations versus shortest distances to source fault (lower). Red solid and dotted curves show the empirical PGA attenuation distance relationship for surface data by Si and Midorikawa (1999) and its standard deviation

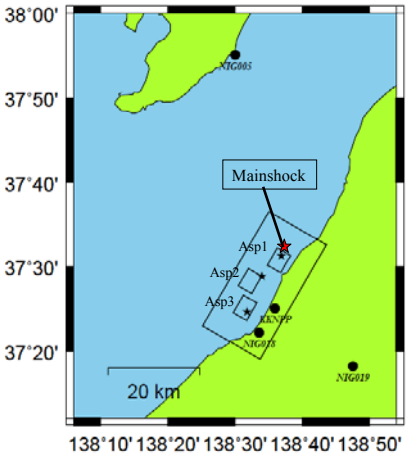

Figure 6 Map showing source model (rectangular) consisting of three asperities (Asp1, Asp2 and Asp3) in this study and the locations of K-net stations and KKNPP (circle) and the epicenter of the mainshock (red star).

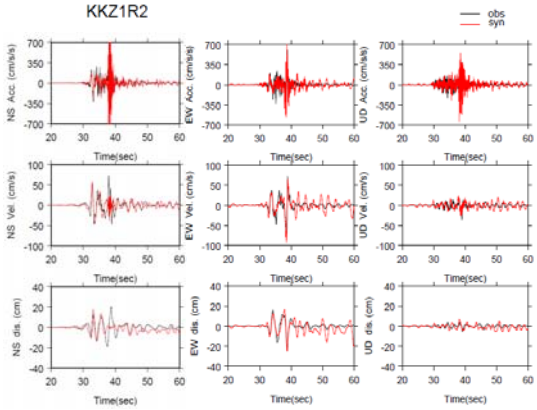

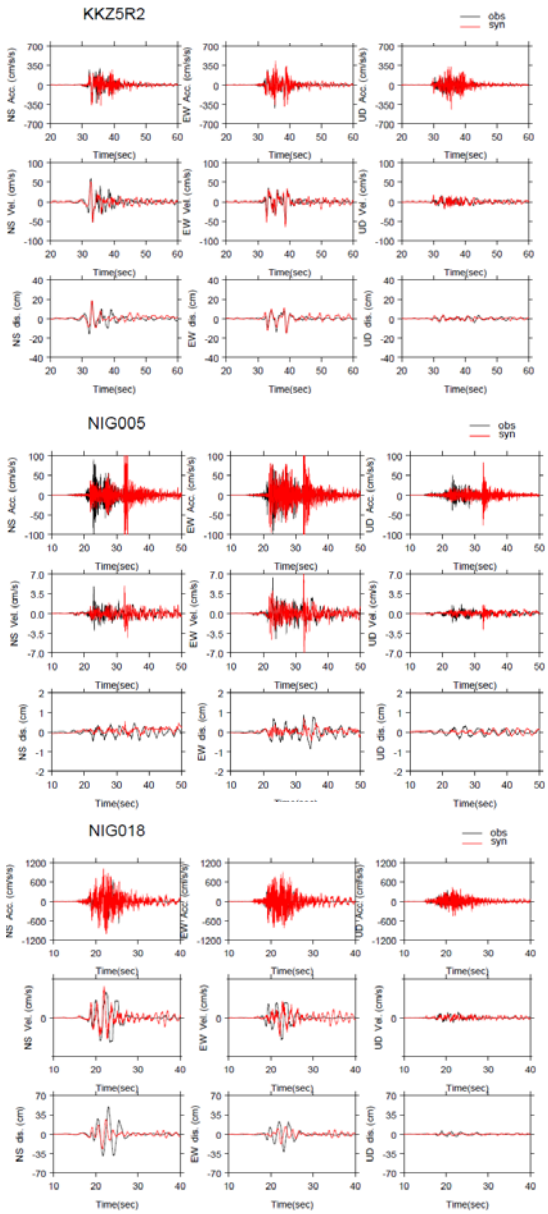

Figure 7 Comparison between the observed records (black) and synthesized motions (red). Acceleration (top), velocity (middle) and displacement (bottom) are shown at KKZ1R2, KKZ5R2, NIG005 and NIG018.

3.2 Verification of the "Recipe" for Recent Disastrous Earthquakes

We introduce two more examples, one is the 2007 Noto Hanto earthquake and the 2005 Fukuoka-ken Seiho-oki earthquake.

The 2007 Noto-Hanto earthquake (Mw=6.7) on March 25, 2007 occurred west off the Noto peninsula, Japan in Fig. 8. Strong ground motions with the JMA seismic intensity of 6-upper struck Wajima, Anamizu, and Nanao in the northern part of the Noto peninsula. The PGA's of this earthquake with shortest fault distance seem to be a little larger than the empirical attenuation-distance relationships by Si and Midorikawa (1999) as shown in Fig. 9.

The source slip model of the 2005 Noto Hanto

earthquake was determined from the inversion of strong ground motion records by Horikawa (2007). His result is not always available for strong motion simulation because the inversion is done using only long-period motions more than 1 sec. The characterized source model with asperities inside the rupture area is needed to simulate broadband motions including short-period motions less than 1 sec. for accurate estimation of seismic intensity interest. The asperities are defined as rectangular regions where the slip exceeds in the same specified manner as Somerville et al. (1999). Resultant source model is shown in the left of Fig. 10. For comparison, we made a source model following the "recipe" as shown in the middle of Fig. 10, where the asperity area and stress parameters are estimated from the acceleration source spectral-level of observed data.

Further, we made a source model by forward modeling, comparing between the observed records and synthesized motions based on the characterized source model using the empirical Green's function method. The best-fit source model consists of two asperities with different size shown in Fig. 10. A large one is located just above the hypocenter with an area of 6.3 x 6.3 km^2 and stress drop of about 26 MPa. A smaller one is located north-east of the large one with an area of 3.6 x 3.6 km^2 and stress drop of about 10 MPa. The stress drops of the asperities are about two times higher than average values of inland crustal earthquakes so far estimated.

The outer and inner fault parameters of those three source models (waveform inversion, recipe and forward modeling) are summarized in Table 4 and 5, respectively. The stress drop of the asperity estimated from the waveform inversion is almost the same as those from the recipe. However, the asperities by the forward modeling have a little larger stress drop (ASP1:26MPa) than the empirical ones. This result is consistent with lager acceleration than the empirical attenuation distance relation in Fig. 9.

Observed motions at ISK001 and ISK003 are compared with synthesized motions for those three source models in Fig. 11. The synthesized waveforms for any models almost agree with the observed ones. Of course, the forward modeling gave the synthesized motions best-fit to the observed.

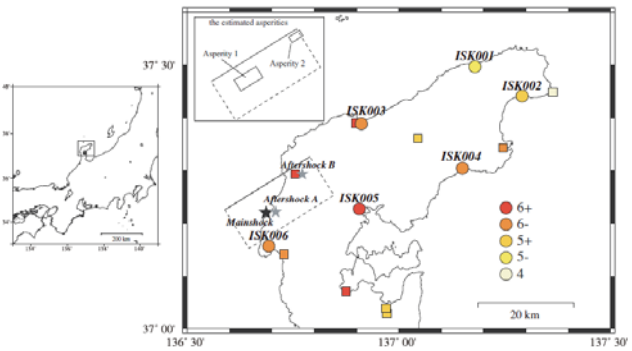

Figure 8 Map showing source fault of 2007 Noto Hanto earthquake (rectangular), the locations of stations used for analysis (circle), the other stations (square) and epicenter of the mainshock (star).

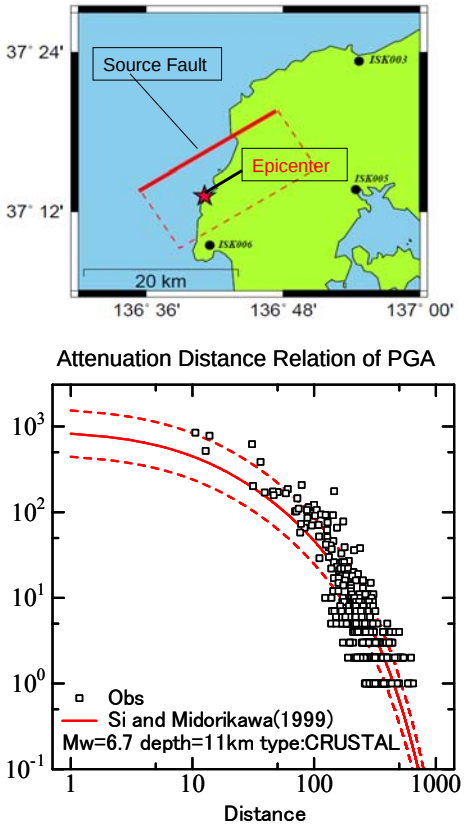

Figure 9 Upper: Map showing source fault by Horikawa (2007). Lower: Relationship of observed peak horizontal ground accelerations versus shortest distances to the source fault. Red solid and dotted curves show the empirical PGA attenuation distance relationship for surface data by Si and Midorikawa (1999) and its standard deviation (lower).

Table 4 Source parameters for slip model of the Noto-hanto earthquake estimated with the wave inversion using strong ground motions by Horikawa (2007).

Strike	Dip	Length	Width	Area
58	60	22km	20km	440km^2
Seismic Moment		Static Stress Drop		
1.08E+19 Nm		2.84 MPa		

Table 5 Source parameters for the characterized source model by three models.

	Waveform Inversion	Recipe	Forward Modeling
Total Area S (km^2)	90	90.6	52.65
Sa/S	20.45	20.59	11.97
Source Radius (km)	5.35	5.37	4.09
Seismic Moment (Nm)	4.41E+18	4.43E+18	2.90E+18
Stress Drop (MPa)	13.9	13.8	ASP1 : 26
			ASP2 : 10

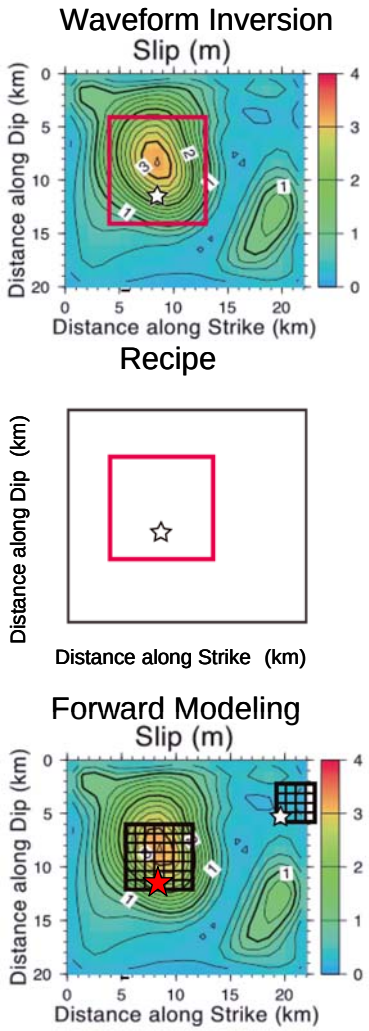

Figure 10 Characterized source models with asperities inside the rupture area. Upper is a model by waveform inversion result, Middle is that by recipe, and Bottom is that by forward modeling.

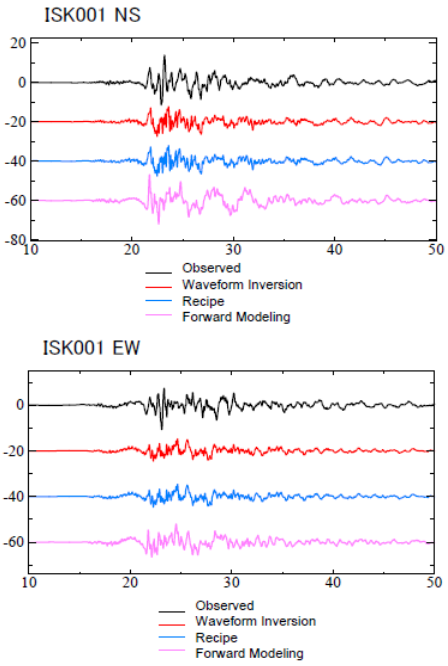

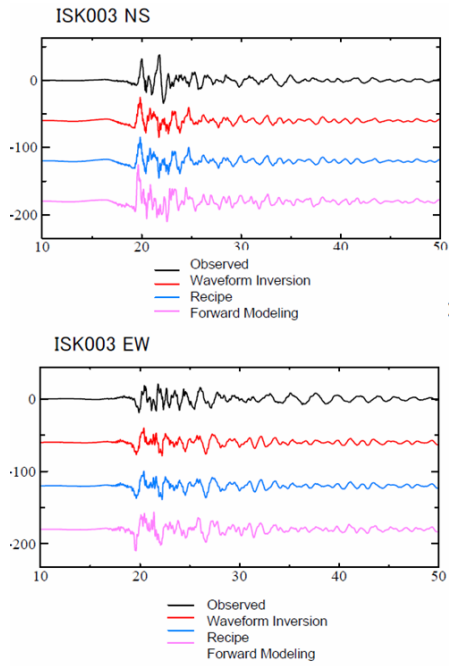

Figure 11 Comparison between observed records and synthesized motions for three source models by waveform inversion, recipe, and forward modeling at ISK001 and ISK003.

The 2005 Fukuoka-ken Seiho-oki earthquake (Mw=6.6) on March 20, 2005 occurred west off the Fukuoka peninsula, Japan. The fault plane projected to surface and observation sites are shown in Fig. 12. The source slip model of this earthquake was determined from the inversion of strong ground motion records by several authors (e.g. Kobayashi et al. 2006, Sekiguchi et al. 2006, Asano et al. 2006, and so on). The slip distribution on the fault plane is roughly similar each other, although there are some differences depending on frequency ranges of the data, smoothing techniques used there and etc. Even if the inverted source model is almost uniquely determined, it is not always available for strong motion simulation. Those inversions were done using only long-period motions more than 1 sec.

Verification of estimating strong ground motions for this earthquake based on "recipe" was made by Earthquake Research Committee (2007). We describe the outline of the verification mentioned above.

The characterized source model with asperities inside the rupture area is needed to simulate broadband motions including short-period motions less than 1 sec. for accurate estimation of seismic intensity interest. The asperities are defined as rectangular regions where the slip exceeds in the same specified manner as Somerville et al. (1999).

Three source models, Case 1, 2, and 3 are made for slip models inverted from strong motion data by Kobayashi et al. (2006), Sekiguchi et al. (2006), Asano et al. (2006) as shown in Fig. 13 (Strong Motion Evaluation Committee 2007). Another source model Case 4 is added following the "recipe". The locations of those three asperities are set referring the results from the other inverted models. The

combined areas of asperities and the stress parameters for the inverted source models are 48 ~ 64 km^2 and 20 ~26 MPa, while those of the recipe model are 80 km^2 and 16 MPa, respectively. That is, in the recipe model the asperity is a little wider and the stress parameter is somewhat small.

The synthesized motions are calculated using a hybrid method (Irikura and Kamae 1999) with the crossover period of 1 sec, summing up longer period motions with a theoretical procedure and shorter period motions with the stochastic Green's function method. Synthesized velocity waveforms at engineering bed rock are compared with the observed ones at 10 sites in Fig. 14. We found that the synthesized motions agree well with the observe records, although the synthesized ones at some sites are a little smaller because the effects of surface geology are not considered.

We compiled the relationship between the combined areas of the asperities and total seismic moments for earthquakes so far analyzed in Fig. 15. The recent disastrous earthquakes introduced here almost follow the empirical relationship so far reported. Speaking more detailed, the asperity areas of the 2007 Noto Hanto earthquakes have a little smaller than those of the 2007 Chuetsu-oki earthquake, resultantly related to higher stress parameters on asperities and larger accelerations.

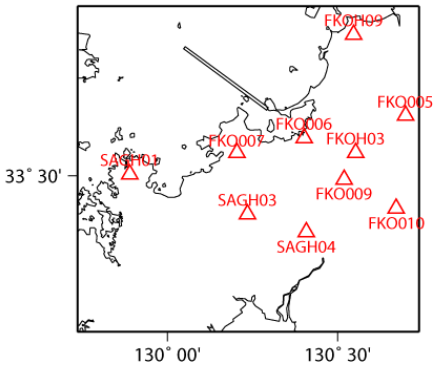

Figure 12 Map showing fault plane (rectangular) and the location of stations used for analysis (triangles).

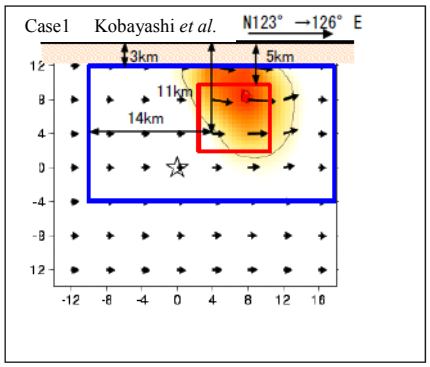

Figure 13 Four characterized source models (Case 1, Case 2, Case 3, Case 4) with asperities inside rupture area. Case 1 to 3 are from inversion results by Kobayashi et al. (2006), Asano et al. (2006), and Sekiguchi et al. (2006), respectively.

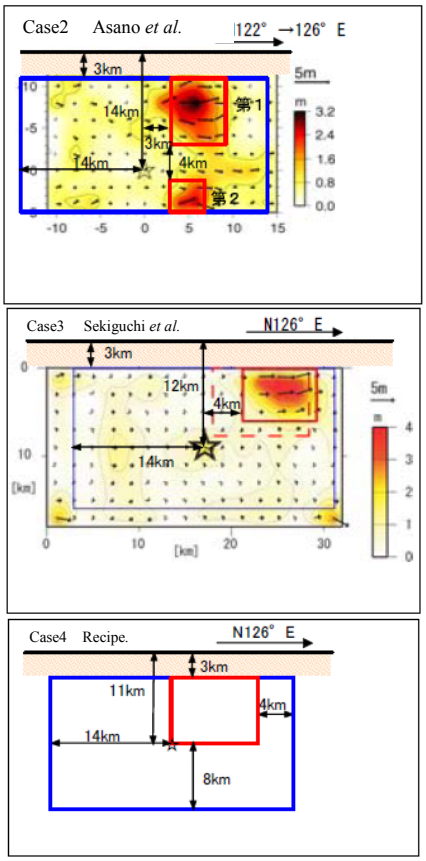

Figure 13 Continued.

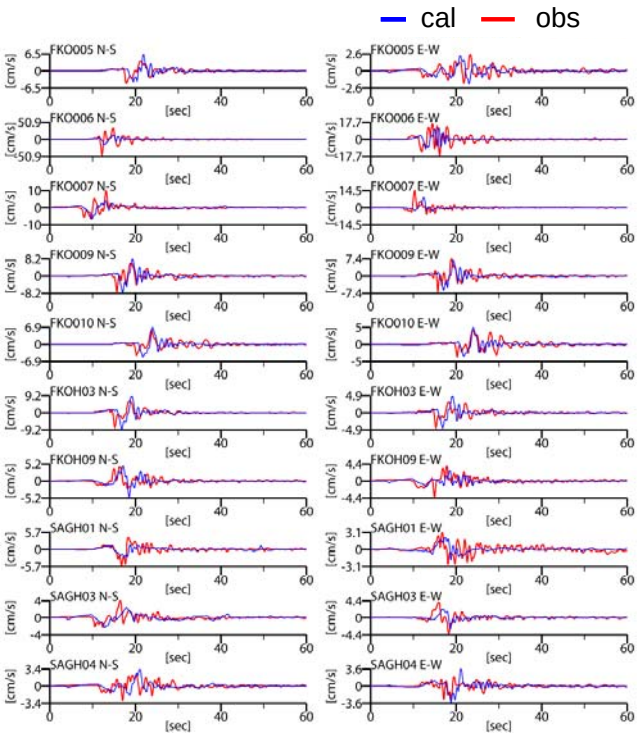

Figure 14 Comparison between observed records (red) and synthesized motions by a hybrid method (blue) at 10 stations.

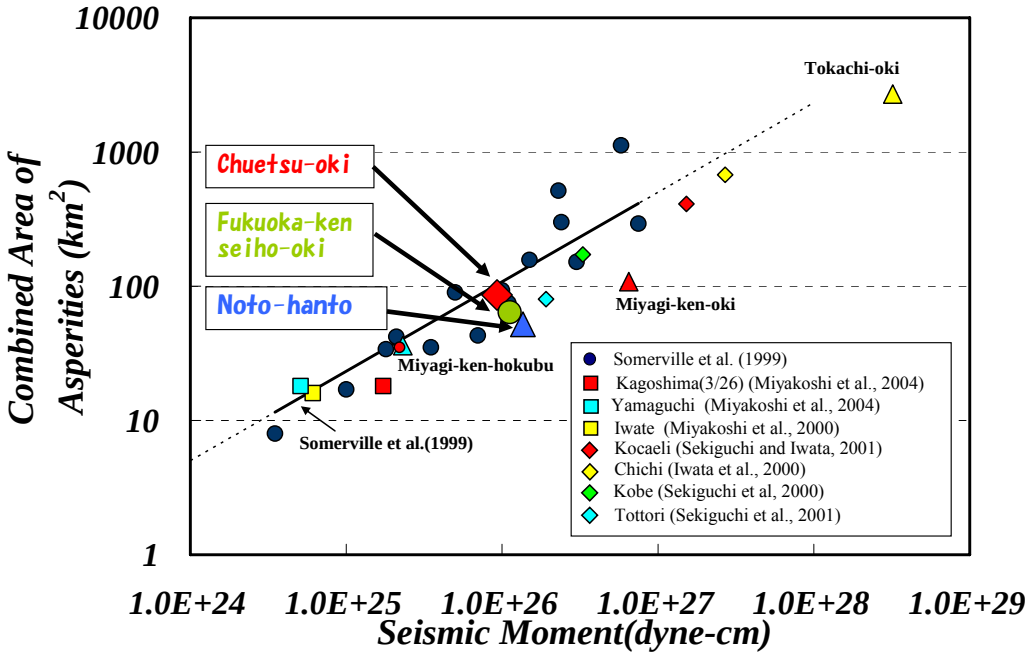

Figure 15 Relationship between combined areas of asperities and total seismic moments for earthquakes.

4. OVERVIEWS OF STRONG MOTION PREDICTIONS

One of the problems with strong motion maps is that recent disastrous earthquakes have occurred in regions where probability of ground motions is relatively small, for example, 2000 Tottori-ken Seibu earthquake, 2004 Chuetsu earthquake, 2005 Fukuoka-ken Seiho-oki earthquake, 2007 Noto-hanto earthquake, 2007 Chuetsu-oki earthquake. Therefore, the maps by themselves are not always responsible for people who expect seismologists and earthquake engineers to reduce earthquake damage for future large earthquakes.

These earthquakes are caused to inland and offshore active folds and faults. A reason is that high shaking areas in probabilistic sense are related to mainly subduction earthquakes, because probability of earthquake occurrence on inland active folds and faults are one order smaller than inland crustal earthquakes. It comes from lack of data for so far for active fault information on offshore. The Headquater of Earthquake Research Promotion has made evaluation of long-term earthquake predictions only for active faults and fault systems on land, but not on offshore. They have not systematically surveyed active tectonics on offshore. We need to promote such seismo-tectonics studies in offshore regions, source modeling for active folds as well as active fault systems, and strong motion predictions for potential earthquakes.

Another problem is associated with earthquake safety of important structure, in particular nuclear power plants.

The two earthquakes, 2007 Noto-hanto and 2007 Chuetsu-oki earthquakes happened very close to the Nuclear Power Plants and stroke extremely strong ground motions more than the levels accounted for in the aseismic design of the plants. In particular, ground motions from the Chetsu-oki earthquake exceeded 2.5 times of the design level. Although the level of the seismic input in the design of the plant was exceeded during the earthquake, "there is no visible significant damage because of the conservatisms introduced at different stages of the design process" as the IAEE report says. They also indicated that "a re-evaluation of the seismic safety for Kashiwazaki-Kariwa plant needs to be done with account taken of the lessons learned from the Chuetsu-oki earthquake and using updated criteria and methods." The re-evaluation of the seismic safety should also be done for all of other nuclear power plant in Japan. Detailed geo-morphological, geological, and geophysical investigations have to be made both on land and offshore for defining seismic input motions following revised regulatory guide fro aseismic design of nuclear power plants issued in September 2006. We have not to miss any earthquakes that jeopardize the safety of plants, investigating the potential existence of active faults near plants. To do that, it is necessary to establish methodology of reliable prediction of strong ground motions for earthquakes occurring underneath sites where active faults have not been specified.

Acknowledgements:

We appreciate National Research Institute for Earth Science and Disaster Prevention (NIED) for providing the K-NET, KiK-net and F-net data. We also thank to Tokyo Electric Power Company (TEPCO) for providing strong ground motion data at the Kashiwazaki-Kariwa nuclear power plant.

References:

Asano, K. and Iwata, T. (2006), "Source process and near-source ground motions of the 2005 West Off Fukuoka Prefecture earthquake," *Earth Planets Space,* **58** (1), pp. 93-98.

Dan, K., Watanabe, T., Sato, T. and Ishii, T. (2001), "Short-period source spectra inferred from variable-slip rupture models and modeling of earthquake fault for strong motion prediction," *Journal of Struct. Constr. Engng. AIJ,* **545**, pp. 51-62.

Day, S. M. (1982), "Three-dimensional simulation of spontaneous rupture: the effect of nonuniform prestress," *Bull. Seism. Soc. Am.,* **88**, pp. 512-522.

Earthquake Research Committee (2005), Report: 'National Seismic Hazard Map for Japan (2005), *MEXT, http://www.jishin.go.jp/main/ index-e.html* .

Strong Motion Evaluation Research Committee (2007), "Verification of strong motion evaluation using observed records of the 2005 Fukuoka-ken Seiho-oki Earthquake (in Japanese)", *MEXT, http://www.jishin.go.jp/main/kyoshindo/07mar_fukuoka / index.htm.*

Earthquake Research Institute, Univ. of Tokyo (2008), "The aftershock distribution of 2007 Chuetsu-oki earthquake re-determined using the OBS seismometers," *Report published by Earthquake Research Committee 2008,* (in Japanese).

Eshelby, J. D. (1957), "The determination of the elastic field of an ellipsoidal inclusion, and related problems," *Proc. Roy Soc.,* **A241**, pp. 376-396.

Fujii, Y. and Matsu'ura, M. (2000), "Regional difference in scaling laws for large earthquakes and its tectonic implication," *PAGEOPH,* **157**, pp. 2283-2302.

Fukushima, Y. and Tanaka, T. (1990), "A new attenuation relation for peak horizontal acceleration of strong earthquake ground motion in Japan," *Bull. Seism. Soc. Am.,* **80**, pp. 757-783.

Hikima, K. and Koketsu, K. (2007), "Source process of the 2007 Chuetsu-oki Earthquake Inferred from far field waveforms and strong motions," *Programme and Abstracts for the Seismological Society of Japan, 2007 Fall Meeting,* P1-085, Poster. (in Japanese).

Horikawa, H. (2007), "Source rupture process of 2007 Noto-Hanto Earthquake,"*http://unit.aist.go.jp/actfault/katsudo/jishin/notohanto/hakaikatei2.htm.* (in Japanese).

IAEA (2007), IAEA Mission Report "Preliminary Findings and Lessons Learned from the 16 July 2007 Earthquake at Kashiwazaki-Kariwa NPP" Vol. I., http://www.nisa.meti.go.jp/english/index.htm.

Irikura, K. (2004), "Recipe for predicting strong ground motion from future large earthquake," *Annuals of Disaster Prevention Research Institute.,* **47A**, pp. 25- 45. (in Japanese).

Irikura, K. and Kamae, K. (1999), "Strong ground motions during the 1948 Fukui earthquake," *Zisin,* **52**, pp. 129-150. (in Japanese with English abstract).

Irikura, K. and Miyake, H. (2001), "Prediction of strong ground motions for scenario earthquakes," *Journal of Geography,* **110**, pp. 849-875 (in Japanese with English abstract).

Irikura, K. and H. Miyake (2002). Source modeling for strong ground motion prediction, *Chikyu, Monthly*, extra issue **37**, 62‐77 (in Japanese).

Kame, N. and Yamashita, T. (2003), "Dynamic branching, arresting of rupture and the seismic wave radiation in self-chosen crack path modeling," *Geophys. J. Int.,* **155**, pp. 1042-1050.

Kanamori, H. and Anderson, D. L. (1975), "Theoretical basis of some empirical relations in seismology," *Bull. Seism. Soc. Am.,* **86**, pp. 1073-1095.

Kobayashi, R., Miyazaki, S. and Koketsu, K. (2006), "Source processes of the 2005 West Off Fukuoka Prefecture earthquake and its largest aftershock inferred from strong motion and 1-Hz GPS data," *Earth Planets Space,* **58** (1), pp. 57-62.

Madariaga, R. (1977), "High frequency radiation from crack (stress drop) models of earthquake faulting," *Geophys. J. R. Astron. Soc.,* **51**, pp. 625-651.

Madariaga, R. (1979), "On the relation between seismic moment and stress drop in the presence of stress and strength heterogeneity," *J. Geophys. Res.,* **84**, pp. 2243-2250.

Miyake, H., Iwata, T. and Irikura, K. (2001), "Estimation of rupture propagation direction and strong motion generation area from azimuth and distance dependence of source amplitude spectra," *Geophys. Res. Lett.,* **28**, pp. 2727-2730.

Miyake, H., Iwata, T. and Irikura, K. (2003), "Source characterization for broadband ground-motion simulation: Kinematic heterogeneous source model and strong motion generation area," *Bull. Seism. Soc. Am.,* **93**, pp. 2531-2545.

Morikawa, N. and Fujiwara, H. (2003), "Source and path characteristics for off Tokachi-Nemuro earthquakes," *Programme and Abstracts for the Seismological Society of Japan, 2003 Fall Meeting,* **104**. (in Japanese).

Nakata, T., Shimazaki, K., Suzuki, Y. and Tsukuda, E. (1998), "Fault branching and directivity of rupture propagation," *Journal of Geography,* **107**, pp. 512-528. (in Japanese).

NISA (2007), "The Earthquakes in Niigata Prefecture and its Effects on Kashiwazaki-Kariwa Nuclear Power Station, http://www.nisa.meti.go.jp/english/index.htm.

Satoh, T. (2004), "Short-period spectral level of intraplate and interplate earthquakes occurring off Miyagi prefecture," *Journal of JAEE'2004.,* **4**, pp. 1-4. (in Japanese with English abstract).

Scholz, C. H. (2002), "The mechanics of earthquakes and faulting," *Cambridge University Press.*

Sekiguchi, H., Aoi, S., Honda, R., Morikawa, N., Kunugi, T. and Fujiwara, H. (2006), "Rupture process of the 2005 west off Fukuoka prefecture earthquake obtained from strong motion data of K-NET and KiK-net," *Earth Planets Space,* **58** (1), pp. 37-43.

Si, H. and Midorikawa, S. (1999), "New attenuation relationships for peak ground acceleration and velocity considering effects of fault type and site condition," *J. Struct. Constr. Eng., AIJ.,* **523**, pp. 63-70. (in Japanese with English abstract).

Somerville, P. G., Irikura, K., Graves, R., Sawada, S., Wald, D., Abrahamson, N., Iwasaki, T., Kagawa, T., Smith, N. and Kowada, A. (1999), "Characterizing crustal earthquake slip models for the prediction of strong ground motion," *Seism. Res. Lett.,* **70**, pp. 59-80.

Chapter 3: Source Modeling and Strong Ground Motion Simulation the 2007 Niigata-ken Chuetsu-oki Earthquake (Mj 6.8) in Japan

SOURCE MODELING AND STRONG GROUND MOTION SIMULATION OF THE 2007 NIIGATAKEN CHUETSU-OKI EARTHQUAKE (Mj=6.8) IN JAPAN

Katsuhiro KAMAE[1] and Hidenori KAWABE[2]

[1] *Professor, Research Reactor Institute, Kyoto University, Osaka, Japan*
[2] *Assistant Professor, Research Reactor Institute, Kyoto University, Osaka, Japan*
Email: kamae@rri.kyoto-u.ac.jp, kawabe@rri.kyoto-u.ac.jp

ABSTRACT :

The Niigataken Chuetsu-oki earthquake (M_j=6.8) occurred on July 16, 2007, northwest-off Kashiwazaki in Niigata prefecture, Japan. In this earthquake, severe damages of fifteen people dead, about 1319 collapsed houses and so on around Kashiwazaki have been caused. In particular, strong ground motions struck the Kashiwazaki and Kariwa nuclear power plant (hereafter KK-site), and triggered a fire at an electric transformer and other troubles. although the all nuclear reactors in operation shut down safely and the damages fortunately appeared less than expected from the seismic design level by the design safety margin. The source mechanism of this earthquake is a reverse fault with the fault plane of SW-NE strike and SE dip. In this study, we tried to construct the source model by the forward modeling approach using the empirical Green's function method. Finally, we proposed the best model consisting of three asperities on the fault. In particular, we pointed out the significant pulse observed at KK-site was generated from the asperity located SW direction of the site and amplified by the folded underground structure between the asperity and the site region though the 3-D finite difference computation.

KEYWORDS: source modeling, Niigataken Chuetsu-oki earthquake, strong ground motion, empirical Green's function method, 3-D simulation

1. INTRODUCTION

The Niigataken Chuetsu-oki earthquake (M_j=6.8) occurred on July 16, 2007, northwest-off Kashiwazaki in Niigata prefecture, Japan. Severe damages of fifteen people dead, about 1319 collapsed houses and so on around Kashiwazaki have been caused. In particular, strong ground motions struck the Kashiwazaki and Kariwa nuclear power plant (hereafter KK-site), and triggered a fire at an electric transformer and other troubles. although the all nuclear reactors in operation shut down safely and the damages fortunately appeared less than expected from the seismic design level by the design safety margin. The source mechanism of this earthquake is concluded to be a reverse fault with the fault plane of SW-NE strike and SE dip from the aftershock distribution determined by a number of temporal observations including the OBS (ocean bottom seismometer). To reconfirm the seismic safety of the nuclear power plants based on new guidelines for seismic design which had been issued in September, 2006, it is very important to estimate the source process of this earthquake that radiated the strong ground motion at KK-site. From this point of view, we tried to construct the source model by the forward modeling approach using the empirical Green's function method (Irikura, 1986). The advantage of this method is that it includes the propagation path and local site effects and estimates basically broad-band ground motions as long as the aftershock recordings are accurate enough in broad-frequency band. Furthermore, this method is convenient and robust in case of having difficulty in calculating the theoretical Green's functions because of complicated underground structure around the corresponding region. We used the main-shock and the aftershock data by K-NET, KiK-net, F-net of the National Research Institute for Earth Science and Disaster Prevention (NIED), and by Tokyo Electric Power Company (TEPCO) at KK-site. Furthermore, we verified the source model from the 3-D finite difference computation using the complicated folded underground structure model derived from the deep borehole data, reflection wave seismic surveys and so on.

2. STRONG GROUND MOTION DATA

We used broad-band acceleration data at NIG005, NIG016 and NIG025 by K-NET , at NIGH07, NIGH15 and NIGH16 by KiK-net, at KZK by F-net, and at KKZ1R2 and KKZ5R2, which are located at basement in underground of Unit 1 and Unit 5, respectively, in KK-site. The locations of these stations are shown in Fig. 1 together with the epicenters of the mainshock and the aftershock used here as the empirical Green's function. Table 1 and Table 2 show the information of the mainshock and the aftershock, respectively. The source parameters of the aftershock were estimated roughly from the displacement source spectra calculated by the borehole data of KiK-net which are not affected strongly by the reflected wave from the ground surface. We use the mainshock and aftershock data bandpass-filtered 0.2 to 10.0 Hz depending on the quality of the aftershock waveform data.

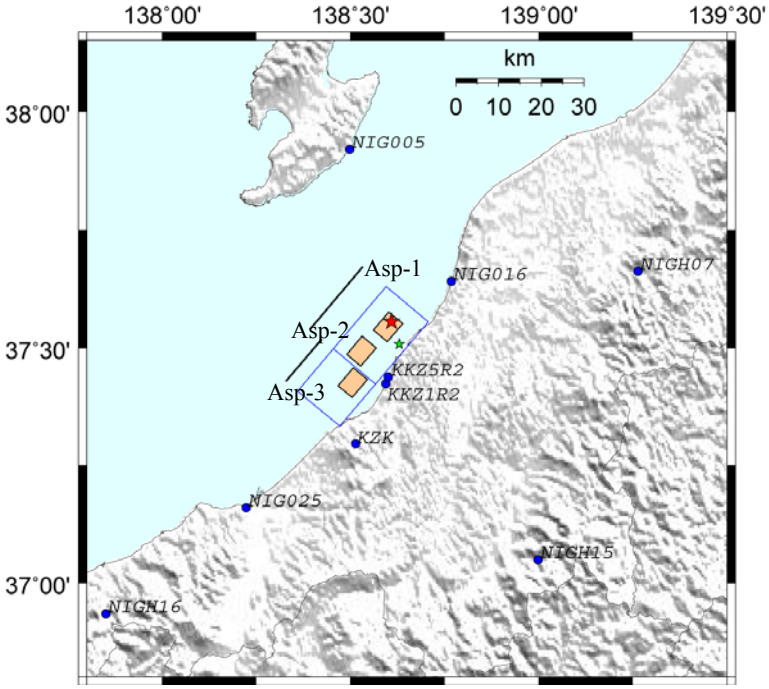

Figure 1 Map showing the location of the epicenters of the mainshock and the aftershock, observation stations and asperities. The red star, green star and blue circles indicate the location of the epicenters of the mainshock, the aftershock, and observation station respectively. The rectangular box depicts the region for the asperities.

Table 1 Information of the mainshock

Origin Time (JST)	2007/7/16 10:13
Latitude (deg)	37.557
Longitude (deg)	138.610
Depth (km)	16.8
M_{JMA}	6.8

Table 2 Source parameters of the aftershock

Origin Time (JST)	2007/7/16 21:08
Latitude (deg)	37.509
Longitude (deg)	138.630
Depth (km)	20.4
M_{JMA}	4.4
Seismic moment (Nm)*	5.21×10^{15}
Focal Mechanism Solution* [Strike/Rake/Dip] (deg)	187/54/70
	39/41/115
Area (km2)	1.4 × 1.4
Stress Drop (MPa)	4.6

* Source parameters estimated by F-net

3. SOURCE MODELING

Several inverted source models have already been proposed from teleseismic data or/and strong ground motion data (Hikima and Koketsu (2008), and Aoi (2008), Nozu (2008)). These models present two or three regions with a relatively large slip – in the part near the hypocenter, one or two parts of south-west direction of the hypocenter –. Firstly, we assumed a simplified source model composed of asperities located on three regions referring to the inverted source models. This assumption is based on the recent studies (i.e. Kamae and Kawabe (2004)) that strong ground motions near source are controlled by the asperities. Finally, we adjusted the locations, sizes, and stress parameters of those three asperities shown in Fig. 1 to fit the simulated motions to the observed ones using a forward modeling approach. In special, we regarded the fitting at KK-site near source as the important. We assumed an S-wave velocity of 3.5 km/s along the wave propagation path and a rupture velocity of 2.7 km/s on the fault plane. Furthermore, we assumed that the rupture should start from red star inside Asp-1 and propagate radially. The ruptures of Asp-2 and Asp-3 restart from each green stars after the rupture reaches each green stars and propagate radially. After several trials, we obtained the best source model shown in Fig. 1 and Fig. 2. The source parameters for each asperity are summarized in Table 3. The stress parameters (stress drop) of these asperities are 1.5- 2.0 times larger than the averaged one (About 12 MPa) for past inland earthquakes (Somerville *et al.*, 1999). As examples, the synthesized motions at KKZ1R2 and KKZ5R2 in KK-site, NIG016 of K-NET and NIGH15 of KiK-net are compared with the observed ones in Fig. 3. Fig. 4 shows the comparison between those synthetic and observed pseudo-velocity response spectra (PVRS) with a damping factor of 0.05. The synthesized waveforms and the PVRS agree with the observed ones fairly well. In particular, separate contributions from each asperity at KKZ1R2 and KKZ5R2 are well produced in the synthesized velocity and displacement waveforms. However, the synthesized ground motion from Asp-3, which is an important and destructive pulsive waveform, is slightly overestimated at KZK5R2 and is estimated well at KZK1R2. Such a discrepancy at both sites might suggested to use more appropriate aftershock data under considering the realistic propagation path effect of the seismic waves from Asp-3.

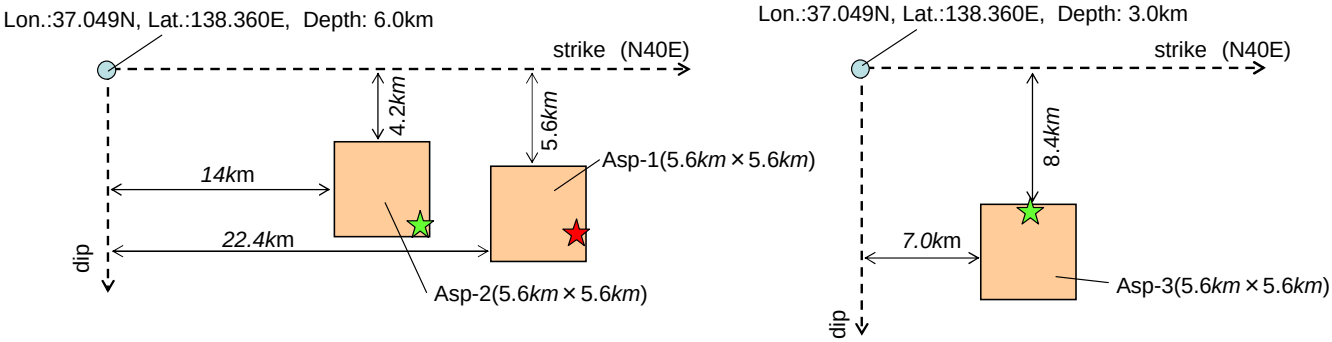

(a) Asp-1 and Asp-2 (b) Asp-3

Figure 2 Source model of the Niigataken Chuetsu-oki earthquake (M_j=6.8). The red star and green stars indicate the location of the epicenter (the rupture start point of Asp-1) and the rupture start points of Asp-2 and Asp-3, respectively.

Table 3 Source parameters of the Niigataken Chuetsu-oki earthquake (M_j=6.8)

	Strike (°)	Dip (°)	Rake (°)	S (km^2)	Mo (Nm)	Δσ (MPa)
Asp-1	40	40	90	5.6 × 5.6	1.33×10^{18}	18.4
Asp-2	40	40	90	5.6 × 5.6	2.00×10^{18}	27.6
Asp-3	40	40	90	5.6 × 5.6	1.67×10^{18}	23.0

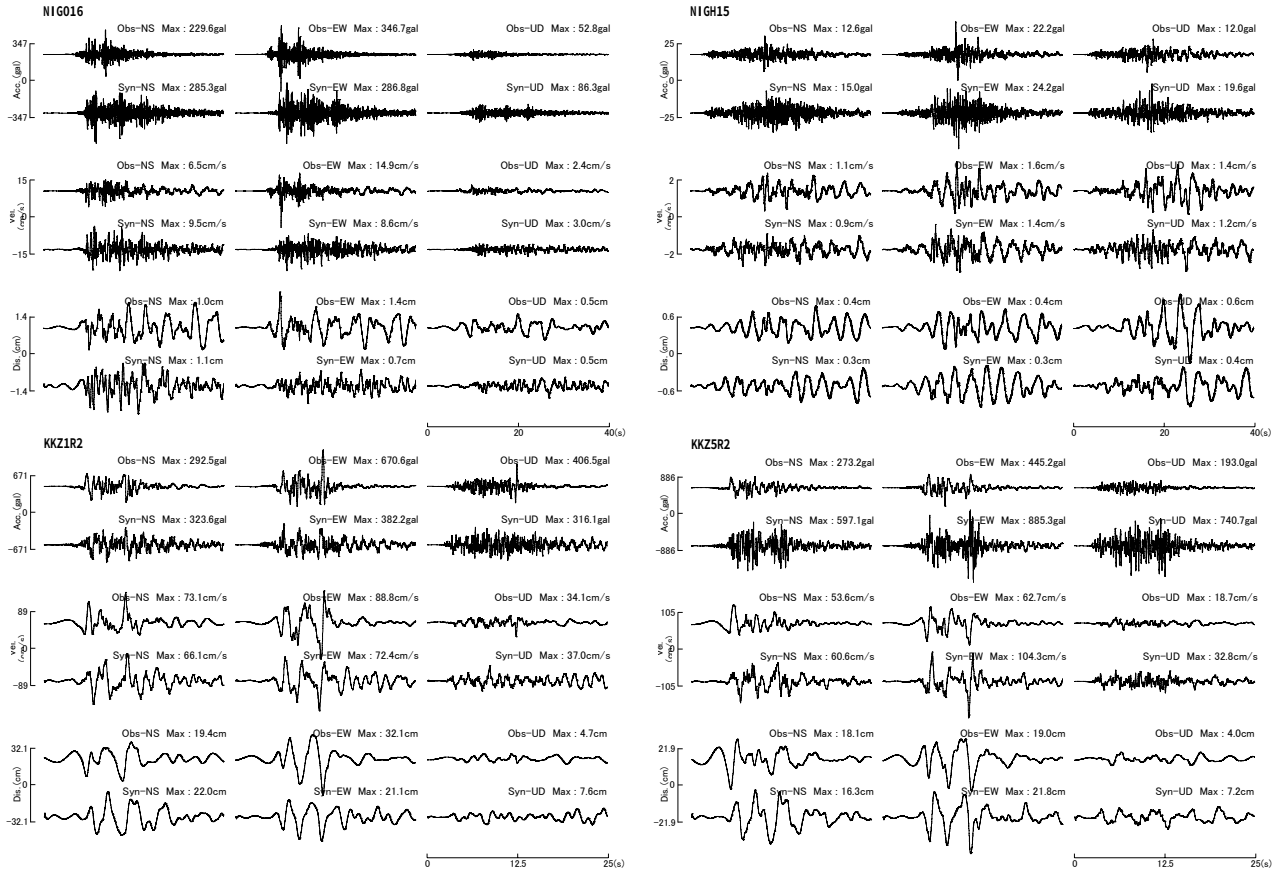

Figure 3 Comparison between the synthesized and observed motions at NIG016, NIGH15, KKZ1R2 and KKZ5R2.

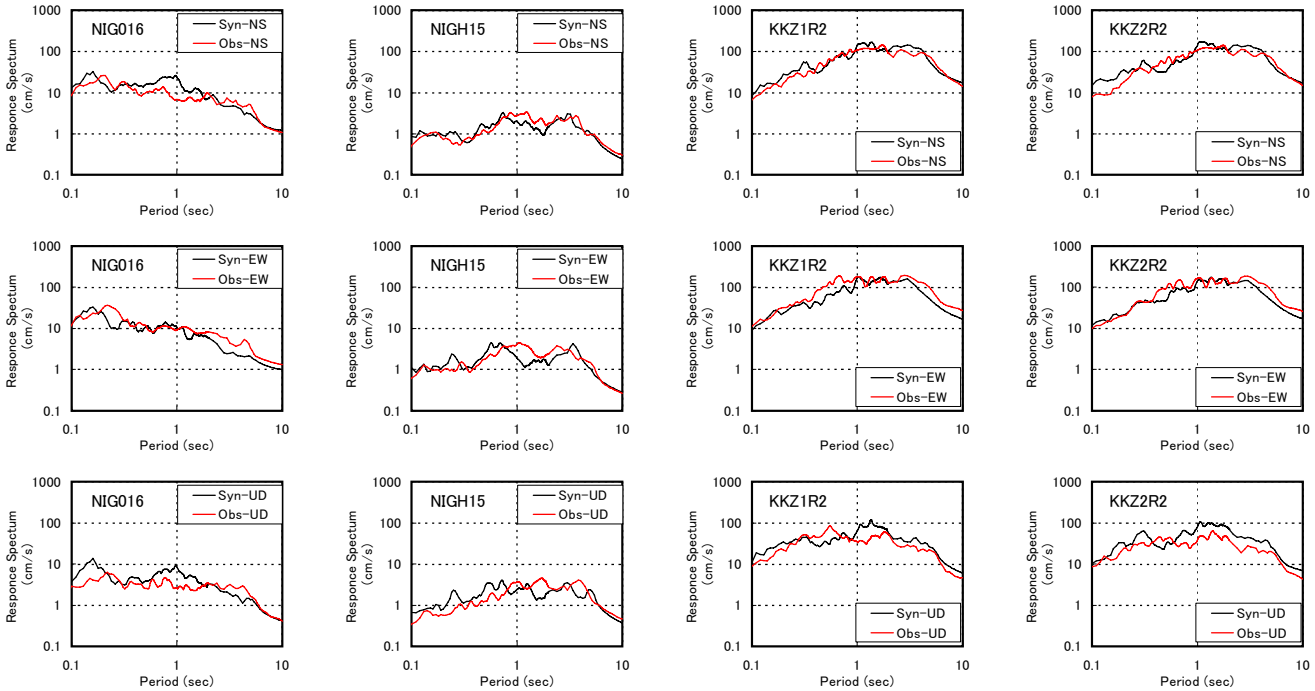

Figure 4 Comparison of the pseudo-velocity response spectra (PVRS) with damping factor of 0.05 of the synthesized motions and those of the observed motions at four sites. Black line shows the PVRS of the synthesized motions. Red line shows the PVRS of the observed motions.

3. 3-D SIMULATION AND DISCUSSION

Ground motion simulations were performed using 3-D finite-difference procedure proposed by Pitarka (1999) to verify the validity of the proposed source model and to investigate why the destructive pulsive waveforms from Asp-3 were generated at KKZ1R2 and KKZ5R2 in KK-site. This simulation algorithm is accurate to fourth order in space and second order in time, and with a non-uniform spacing staggered-grid formulation. We set an absorbing region outside the finite computation region shown in Fig. 5 and applied the non-reflecting boundary condition of Cerjan *et al*. (1985) and the A1 absorbing boundary condition of Clayton and Engquist (1977). The implementation of the attenuation into the method is based on the technique by Graves (1996), which considers Q to be identical and frequency dependent for both P and S waves (Kawabe and Kamae, 2008). The 3D velocity structure used for this region (44.4km×60.0km) is from Japan Nuclear Energy Safety Organization (2005) (2005). This model is composed of several layers with different velocity on basement rock. The depths of each sedimentary layer and basement rock surface are shown in Fig. 6. The parameters of these layers are summarized in Table 4. Fig. 7 illustrates the simulated peak ground velocity (PGV) distribution in a horizontal component (EW). Fig. 8 shows the comparison between the synthesized velocity waveforms and the observed ones in frequency range of 0.05-1.6 Hz at KKZ1R2 and KKZ5R2. Here, you should notice that the synthetics are amplified 1.5 times of the original ones. You can see that the waveforms are simulated fairly well at both stations although the amplitudes are underestimated about 1.5 times comparing with the observed ones because of not including lower velocity layers in the current 3D model. Furthermore, the conspicuous different ground motion amplification from Asp-3 between KZK1R2 and KZK5R2 is not completely reproduced because of the same reason. However, we concluded from Fig. 7 representing the PGV distribution in vertical cross section that this is due to a focusing of seismic wave depending on the folded underground structure in this region. Next, we attempted to investigate quantitatively the 3 dimensional effect at KZK1R2 from the comparison with the one dimensional computation using the discrete wavenumber method (Bouchon, 1981). Fig. 9 shows the comparison of PGV distributions between a couple of the techniques in EW direction passing through KZK1R2. The synthesized PGV at KZK1R2 is amplified about 1.5 times by the 3 dimensional effect. These results suggest the validation of the proposed source model composed of three asperities and the importance of considering a detailed underground structure in strong ground motion predictions.

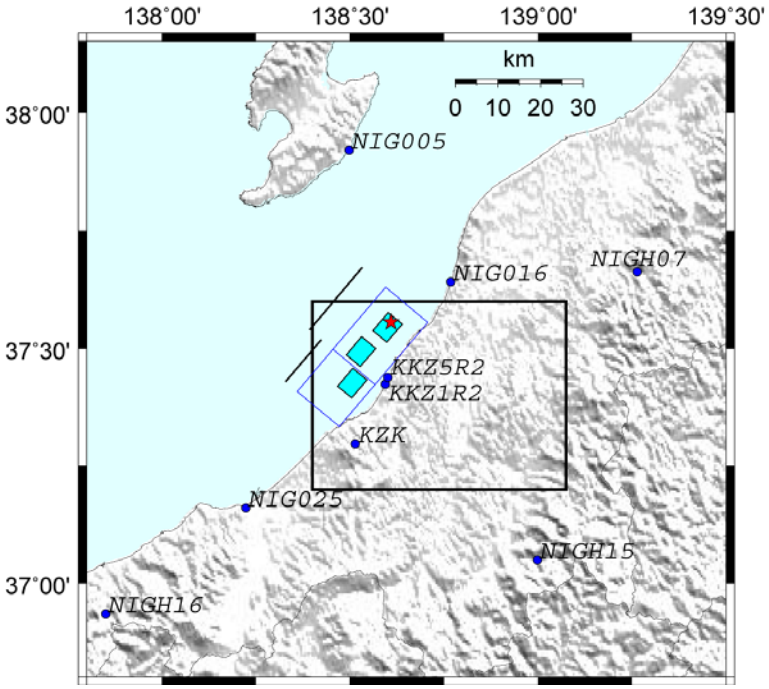

Figure 5 Map showing the location of the epicenter shown in Table 1 and observation stations. The thick rectangular box depicts the region for the 3D finite difference simulation.

Table 4 Parameters of the velocity structure model

Layer No.	density (g/cm^3)	Vs (km/s)	Vp (km/s)
Layer 1	2.05	0.80	2.20
Layer 2	2.20	1.30	2.90
Layer 3	2.25	1.40	3.10
Layer 4	2.35	1.70	3.70
Layer 5	2.40	2.00	4.10
Layer 6	2.50	2.40	4.70
Layer 7	2.65	3.00	5.50
Layer 8	2.70	3.50	5.80

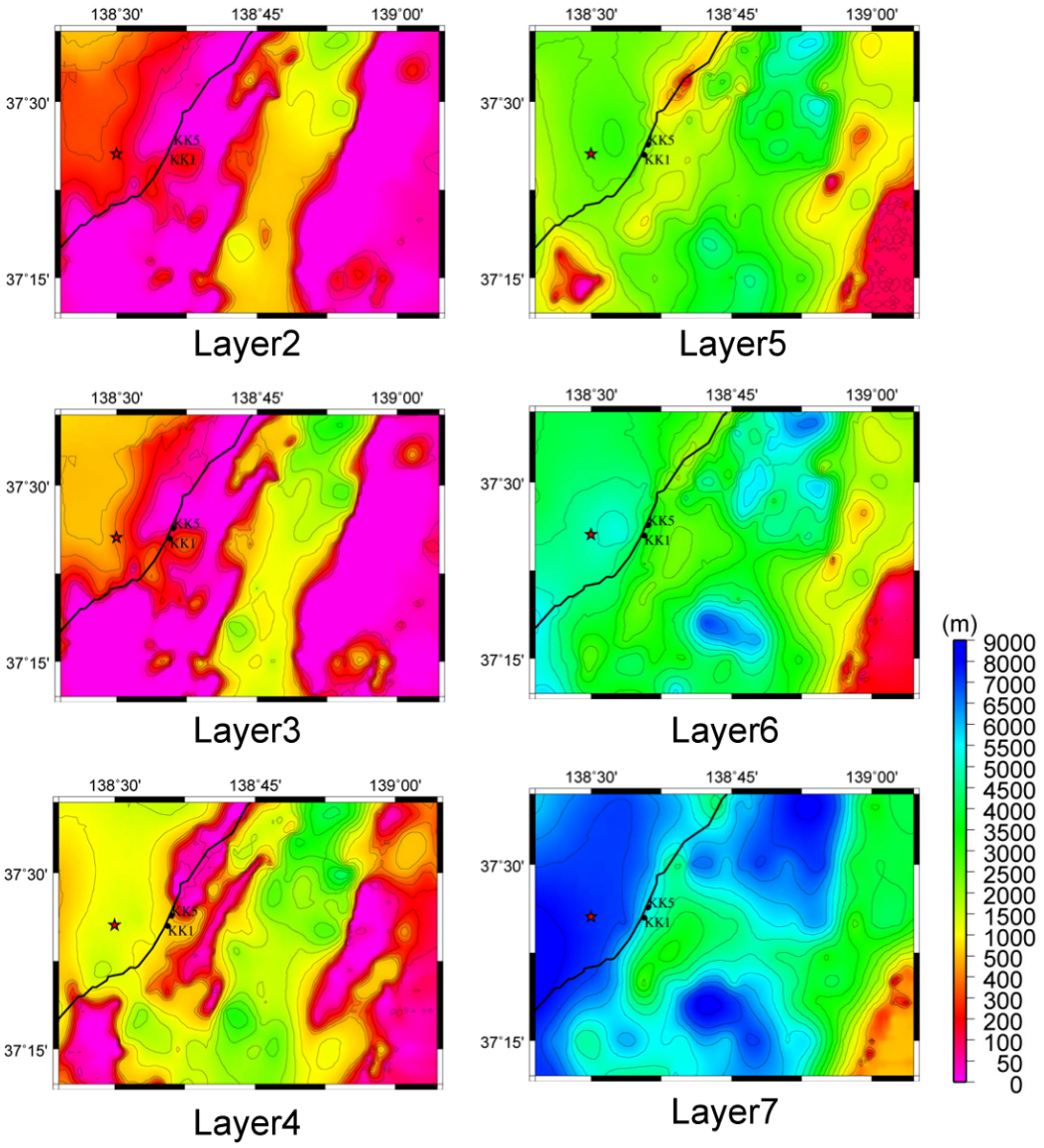

Figure 6 Topography of the bedrock surface and the boundaries between sedimentary layers of the velocity structure model.

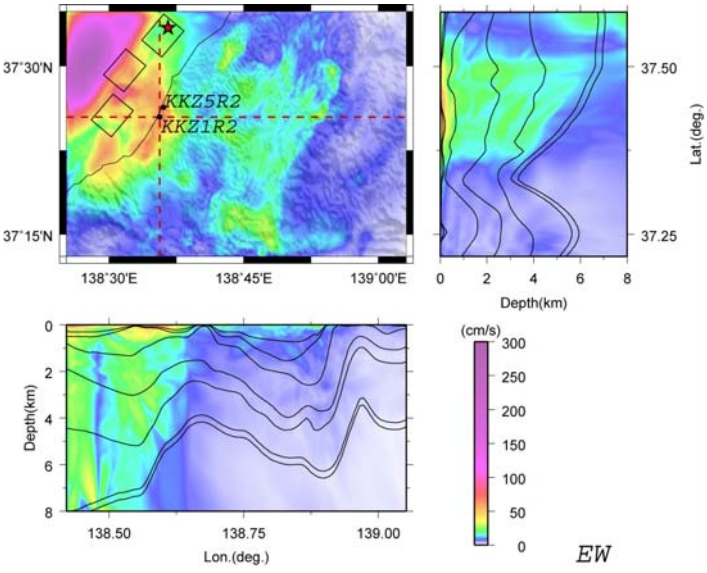

Figure 7 The simulated peak ground velocity (PGV) distribution on surface and in two cross-sections passing through KZK1R2.

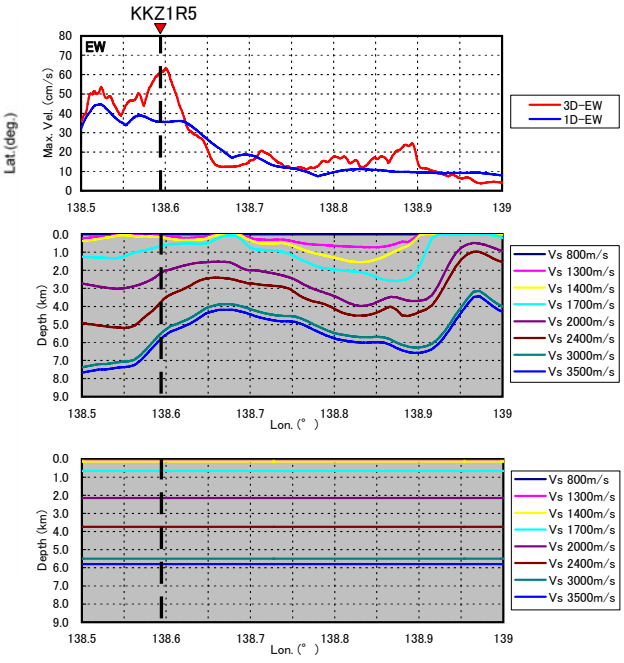

Figure 9 The comparison of PGV distributions between a couple of the techniques in EW direction passing through KZK1R2.

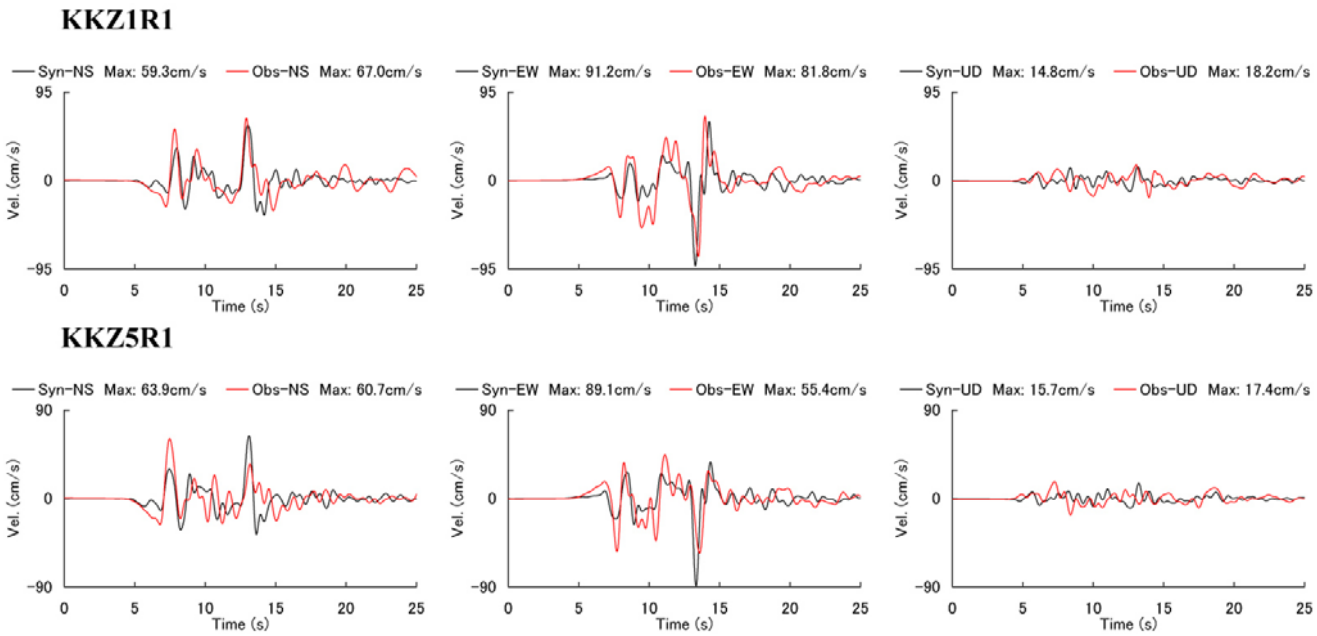

Figure 8 The comparison between the synthesized velocity waveforms and the observed ones in frequency range of 0.05-1.6 Hz.

4. CONCLUSIONS

To investigate why the destructive ground motions were observed at KK-site during the Niigataken Chuetsu-oki earthquake, Japan, we firstly proposed the source model consisting of three asperities on the reverse fault plane with SE dipping by the forward modeling using the empirical Green's function method, secondly verified the validation of the model through some theoretical simulations (3-D and 1-D simulations). We found that the large

amplitude ground motion from Asp-3 lying south-west direction of the KK-site was amplified by the focusing of the seismic wave due to the folded underground structure. A more detailed investigation is needed in simulations using the continuous geological surveys at just KK-site as well as in the corresponding region.

ACKNOWLEDGEMENT

We appreciate National Research Institute for Earth Science and Disaster Prevention for providing us with the K-NET, KiK-net and F-net data. We also thank to Tokyo Electric Power Company for providing us the important acceleration data at KK-site.

REFERENCES

Bouchon, M. (1981). A simple method to calculate Green's functions for elastic layered media. *Bull. Seism. Soc. Am.*, **71**, 959-971.

Cerjan, C., D. Kosloff, R. Kosloff, and M. Reshef (1985). A nonreflecting boundary condition for discrete acoustic and elastic wave equations. *Geophysics*, **50**, 705-708.

Clayton, R. and B. Engquist (1977). Absorbing boundary conditions for acoustic and elastic wave equations. *Bull. Seism. Soc. Am.*, **67**, 1529-1540.

Graves, R.W. (1996). Simulating seismic wave propagation in 3D elastic media using staggered-grid finite differences. *Bull. Seism. Soc. Am.*, **86**, 1091-1106.

Hikima, K. and K. Koketsu (2008). Source process of the 2007 Chuetsu-oki earthquake inferred from far and near field waveforms and geodetic data. Japan Geoscience Union Meeting 2008, S146-015.

Honda, R. and S. Aoi (2008). Back-projection imaging of the 2007 Chuetsu-oki earthquake using strong-motion seismograms observed at a nuclear power plant. Japan Geoscience Union Meeting 2008, S142-002.

Irikura, K. (1986). Prediction of strong acceleration motions using empirical Green's function. *Proc. 7th Japan Earthq. Eng. Symp.*, 151-156.

Japan Nuclear Energy Safety Organization (2005). Study on Seismic Probabilistic Safety Assessment Method =Evaluation of Characteristic of Seismic Motion Based on Identification of Velocity Structure of Deep Soil Configuration=, JNES/SAE05-048. (in Japanese)

Kamae, K. and H. Kawabe (2004). Source model composed of asperities for the 2003 Tokachi-oki, Japan, earthquake (M_{JMA}=8.0) estimated by the empirical Green's function method. *Earth Planets and Space*, **56:3**, 323-327.

Kawabe, H. and K. Kamae (2008). Prediction of long-period ground motions from huge subduction earthquakes in Osaka, Japan. *Journal of Seismology*, **12:2**, 173-184.

Nozu, A. (2008). Evaluation of site amplification factors at Kashiwazaki-Kariwa Nuclear Power Plant and its application to strong motion simulation. Japan Geoscience Union Meeting 2008, S146-016.

Pitarka, A. (1999). 3D elastic finite-difference modeling of seismic wave propagation using staggered grid with non-uniform spacing. *Bull. Seism. Soc. Am.*, **89**, 54-68.

Somerville, P.G., K. Irikura, R. Graves, S. Sawada, D. Wald, N. Abrahamson, Y. Iwasaki, T. Kagawa, N. Smith, and A. Kowada (1999). Characterizing crustal earthquake slip models for the prediction of strong ground motion. *Seismological Research Letters*, **70**, 59-80.

Chapter 4: Damage Prediction of Long-Period Structure during Subduction Earthquakes
–Part1: Long-Period Ground Motion Prediction in the Osaka Basin for Future Nankai Earthquakes -

Damage prediction of long-period structures during subduction earthquakes - Part 1: Long-period ground motion prediction in the Osaka basin for future Nankai Earthquakes -

Hidenori KAWABE[1], Katsuhiro KAMAE[2] and Kojiro IRIKURA[3]

[1] *Assistant Professor, Research Reactor Institute, Kyoto University, Osaka, Japan*
[2] *Professor, Research Reactor Institute, Kyoto University, Osaka, Japan*
[3] *Professor, Disaster Prevention Research Center, Aichi Institute of Technology, Toyota, Japan*
Email: kawabe@rri.kyoto-u.ac.jp, kamae@rri.kyoto-u.ac.jp, irikura@geor.or.jp

ABSTRACT :

The Nankai Trough earthquakes which are subduction earthquakes with magnitude greater than 8 have occurred at intervals of 90 to 150 years. The probability of earthquake occurrence within 30-years from January 1, 2008 are estimated at 60 - 70% and 50 % for the next Tonankai and Nankai earthquakes, respectively, showing very high possibility of the earthquake occurrence. It is very important to predict the long-period ground motions from the next Nankai Trough earthquakes for mitigating their disastrous effects. In this study, we show results of the prediction of future Nankai earthquake in Part 1 and the damage prediction map of high-rise buildings in the Osaka basin in Part 2. This paper (Part 1) focuses on the prediction of the long-period (>2.5s) ground motions in the Osaka basin during future Nankai earthquake using the 3D finite difference method and an earthquake scenario proposed by the Headquarters for Earthquake Research Promotion in Japan. The characteristics of the predicted long-period ground motions for the hypothetical Nankai earthquake are related with the geometry between the source and observation points, and with the thicknesses of the sediments of the basin. The duration of the long-period ground motions in an area located in the central part of the Osaka city is more than 4 minutes, and the largest peak ground velocities (PGVs) exceed 80cm/s. The predominant period is around 6 second. These results indicate the possibility of earthquake damage due to future subduction earthquakes in large-scale constructions such as tall buildings and oil storage tanks in the Osaka area.

KEYWORDS: Long period ground motion, Subduction earthquake, Nankai Trough, Finite difference method

1. INTRODUCTION

Osaka, one of Japan's largest cities, has repeatedly suffered from disasters due to huge subduction earthquakes of magnitude greater than eight occurring along the Nankai Trough. The probability of earthquake reoccurrence within 30 years from January 1, 2008 is very high and estimated at 60–70% and 50% for the next Tonankai and Nankai earthquakes, respectively. Osaka is located inside a basin with thick sediments (about 1 to 3 km), in which long-period ground motions are strongly enhanced during these subduction earthquakes. The generation and growth of such long-period ground motions inside the Osaka basin have been examined by simulations of recordings during the Mj7.1 foreshock of the 2004 off-Kii peninsula earthquake (Yamada and Iwata, 2005). The authors indicated that long-period ground motions inside the basin are amplified and elongated not only by the three-dimensional (3D) underground structure in the basin but also by the sedimentary wedge structure along the Nankai Trough. Many long-period and low-damping structures such as tall buildings, long-span bridges, base-isolated buildings, and oil storage tanks exist inside the Osaka basin. Therefore, it is very important to predict the long-period strong ground motions from the next Tonankai and Nankai earthquakes with moment magnitudes of 8.1 and 8.4, respectively, for mitigating earthquake disasters. In this study, we present the predicted long-period ground motion characteristics inside the Osaka basin during the next Nankai earthquake occurring along the Nankai Trough, which may be of special interest to structural engineers. As a preliminary prediction for the scenario earthquakes, we used the source model from the Headquarters for Earthquake Research Promotion (hereafter, HERP) in Japan. 3D subsurface velocity structure models of the Osaka basin have already been proposed by Kagawa *et al*. (1993), Miyakoshi *et al*. (1999), and Horikawa *et al*.

(2003). These models have been constructed from geophysical and geological data such as from boreholes, seismic reflection surveys, microtremors, and gravity anomaly data. Here, we constructed a modified velocity structure model for the sedimentary basin consisting of three sedimentary layers referring to these existing models, and in 3D calculations, we considered the crustal structure outside the basin as well as the subducting oceanic plate. Finally, we pointed out the possibility of earthquake damage in large-scale constructions due to the predicted long-period ground motions.

2. NUMERICAL METHOD AND 3D VELOCITY STRUCTURE MODEL

In order to predict the long-period ground motions from the next Nankai earthquake, we used a 3D finite difference scheme, with second-order accuracy in time, fourth-order accuracy in space, and with a non-uniform spacing staggered-grid formulation (Pitarka, 1999). We set an absorbing region outside the finite computational region, and applied the non-reflecting boundary condition of Cerjan *et al*. (1985) and the A1 absorbing boundary condition of Clayton and Engquist (1977) to the corresponding region. The implementation of the attenuation into the finite difference method is based on the technique by Graves (1996), which considers Q to be identical and frequency-dependent for both P and S waves (Kawabe and Kamae, 2008). Our 3D velocity structure model consisted of a 3D crustal velocity structure model and a 3D velocity structure model of the Osaka sedimentary basin. The former was constructed based on the crustal velocity structure model (Nakanishi *et al.*, 2002) and the Philippine Sea plate boundary model (Hori *et al.*, 2004). The north–south cross-section of the crustal velocity structure model at longitude 136.375°E is shown in Fig. 1. The continental crust was divided into three layers: the upper crust, lower crust, and mantle wedge. The depths of the top of the lower crust and mantle wedge are 18km and 36km, respectively. The subducting oceanic plate was divided into two layers: an oceanic layer and Philippine slab with thicknesses of 2 and 5 km, respectively. The parameters of the model are summarized in Table 1. The latter model was constructed based on a couple of sedimentary basin models (Miyakoshi *et al.*, 1999; Horikawa *et al.*, 2003) constructed from geophysical and geological data such as boreholes, seismic reflection surveys, microtremors, and gravity anomaly data. Then, the sediment was approximately divided into three layers. The depths of each sedimentary layer and the bedrock surface are shown in Fig. 2. The parameters of the Osaka basin velocity structure model are summarized in Table 2.

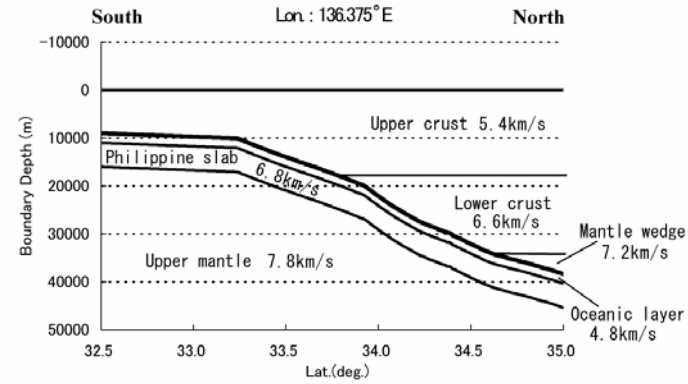

Figure 1 North–south cross-section of the crustal velocity structure model at longitude 136.375°E.

Table 1 parameters of the crustal velocity structure model.

Layer	Vp (km/s)	Vs (km/s)	Density (g/cm^3)
Upper crust	5.4	3.2	2.7
Lower crust	6.6	3.9	2.8
Mantle wedge	7.2	4.3	3.0
Oceanic layer	4.8	2.5	2.6
Philippine slab	6.8	3.9	2.9
Upper mantle	7.8	4.5	3.1

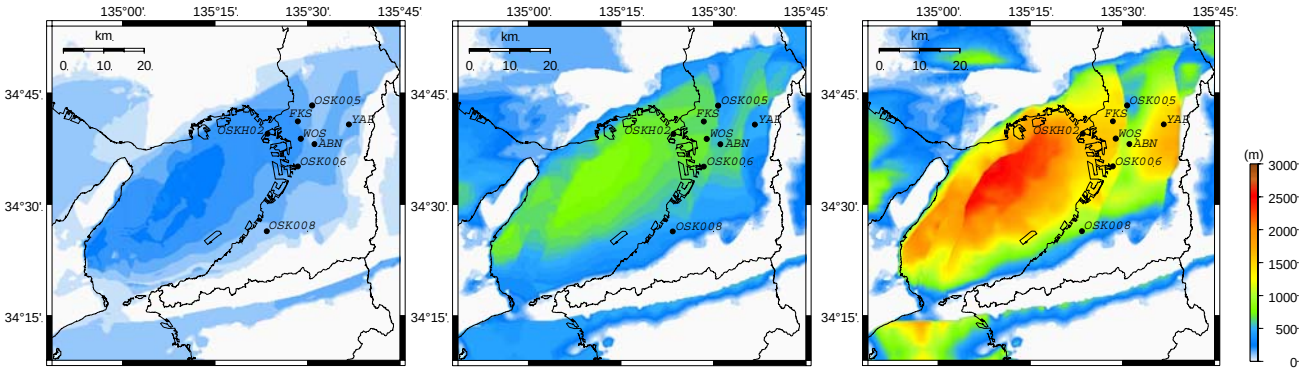

(a) The depth of the boundary between the 1st and the 2nd sedimentary layer.

(b) The depth of the boundary between the 2nd and the 3rd sedimentary layer.

(c) The depth of the boundary between the 3rd sedimentary layer and the bedrock.

Figure 2 Topography of the bedrock surface and the boundaries between sedimentary layers of the Osaka sedimentary basin structure model.

Table 2 Parameters of the Osaka basin velocity structure model.

Layer	Vp (km/s)	Vs (km/s)	Density (g/cm^3)
Sedimentary Layer 1	1.6	0.4	1.7
Sedimentary Layer 2	1.8	0.55	1.8
Sedimentary Layer 3	2.5	1.0	2.1
Bedrock	5.4	3.2	2.7

3. PREDICTION OF LONG-PERIOD GROUND MOTIONS

Here, we attempted to predict long-period ground motions for the next Nankai earthquake using the 3D finite difference method. We used the characterized source models proposed by HERP as the scenarios for the next Nankai earthquake. This model was constructed based on the recipe for estimating strong ground motions from scenario earthquakes provided by Irikura *et al.* (2004). The recipe means the framework for prediction of strong ground motions including the procedures of source modeling, simulation of strong ground motions, and verification of the predicted strong ground motions. The source model is characterized by three kinds of parameters, which are called outer, inner, and extra fault parameters. The outer fault parameters are defined as entire rupture area and total seismic moment for possible earthquake. The inner fault parameters are defined as slip heterogeneity inside the fault area. The extra fault parameters are related to the propagation pattern of the rupture. The outer and inner fault parameters are basically estimated by the scaling relationships derived from statistical analysis of the source inversion results (Somerville *et al.*, 1999). We adopt the slip velocity time function proposed by Nakamura and Miyatake (2000). The location of the source and the region for the 3D finite difference computation are shown in Fig. 3. The locations of the asperities were determined from the backslip model of the Nankai Trough (Nishimura *et al.*, 2000; Zaho and Takemoto, 2000; etc.). Source parameters are summarized in Table 3. The parameters for the 3D simulation of the next Nankai earthquake are listed in Table 4. Fig. 4 illustrates the simulated peak ground velocity (PGV) distributions inside the Osaka basin for the next Nankai earthquake. This figure shows that the PGV distributions drastically change depending on the incident directions of the seismic waves in the basin with complicated underground structure. The PGVs are partially over 80 cm/s inside the Osaka basin. The areas with relative larger amplitude extend along the northern as well as southern basin edges during the next Nankai earthquake. Fig. 5 illustrates the synthesized velocity waveforms at eight stations inside the Osaka basin. The durations of the waveforms are longer than 4 min at almost all stations. Pulsive waveforms appearing at 50–70 s in time are generated by the forward rupture directivity effect due to constant rupture propagation on the asperity (Asp-3). Fig. 6 shows the distributions of pseudo velocity response spectral amplitudes of the expected ground motions in the Osaka basin for the next Nankai earthquake with a damping factor of 5%. This Fig. 9 shows that the predominant

periods of the predicted long-period ground motions can be correlated with the thickness of the sedimentary layers shown in Fig. 1. Fig. 7 illustrates the pseudo velocity response spectra with a damping factor of 5%, together with the safety limit level specified on engineering bedrock, which has an S-wave velocity of about 400 m/s, as the building design regulation in Japan. The predominant periods at almost all stations located on the thicker sedimentary layer are 5–6 s. These predominant periods are supported by recordings during the 2004 off-Kii peninsula earthquake (Miyake and Koketsu, 2005). On the other hand, the predominant periods at stations located on the thinner sedimentary layer close to the basin edges (OSK005 and OSK008) are 3–4 s. These spectral levels exceed the safety limit level described above. Therefore, we can point out the possibility of earthquake damage in large-scale constructions due to the predicted long-period ground motions from the next Nankai earthquake.

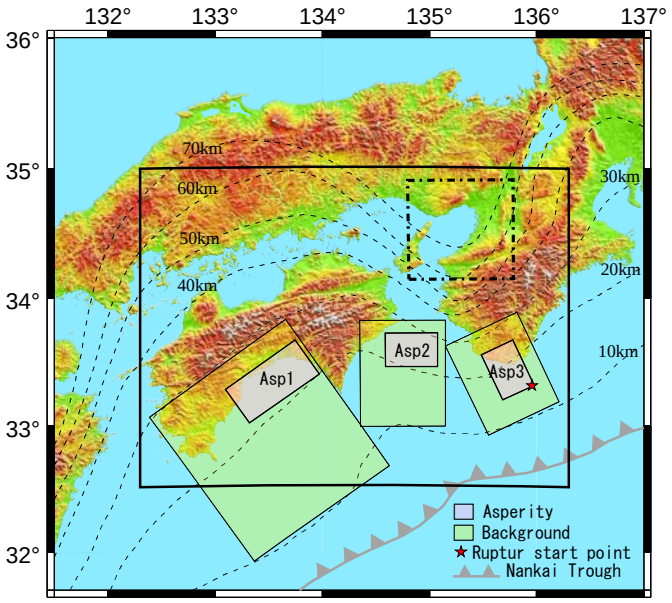

Figure 3 Maps showing the region of western Japan. The thick rectangular box depicts the region for the 3D finite difference simulation of the next Nankai earthquake. The dashed lines indicate the area of the velocity structure model of the Osaka basin. The contours show the isodepth lines of the Philippine Sea plate boundary.

Table 3 Source parameters of the next Nankai earthquake.

Area of source fault (km ^{2})	35800			
Average slip distribution (m)	5.70			
Seismic moment (Nm)	8.34×10^{21}			
Static stress drop (MPa)	3.0			
Rupture velocity (km/s)	3.1			
	1st Asperity (Asp1)	2nd Asperity (Asp2)	3rd Asperity (Asp3)	Background area
Area (km ^{2})	2672	1336	1336	30457
Slip distribution (m)	13.36	9.45	9.45	4.70
Seismic moment (Nm)	1.46×10^{21}	5.16×10^{20}	5.16×10^{20}	5.85×10^{21}
Effective stress drop (MPa)	20.1	20.1	20.1	2.7
Rise time (s)	8.34	5.90	5.90	14.52

Table 4 Model parameters for 3D simulation of the next Nankai earthquake.

Model size	271.8 km × 410.6 km × 84.0 km
Spatial discretization	0.2 km × 0.2 km × 0.1 km (Osaka basin structure model)
	0.6 km × 0.6 km × 0.6 km (Crustal structure model)
Temporal discretization	0.01s
Total time steps	25000

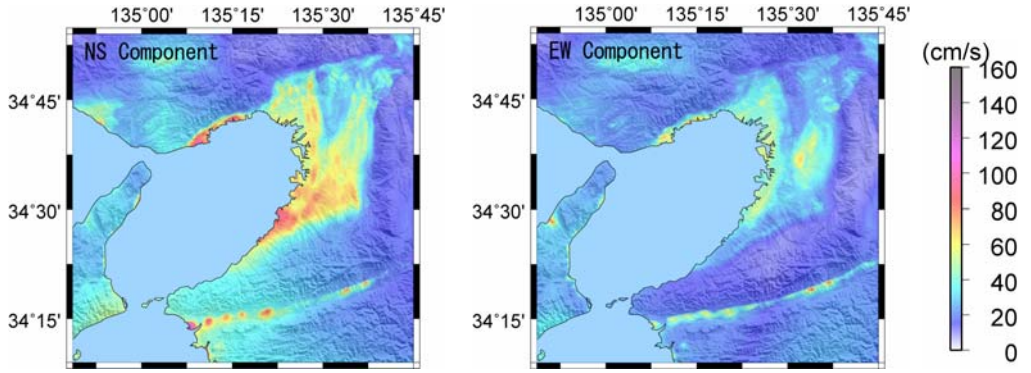

Figure 4 Simulated peak ground velocity distribution for the Nankai earthquake in the Osaka basin (0.05–0.4 Hz).

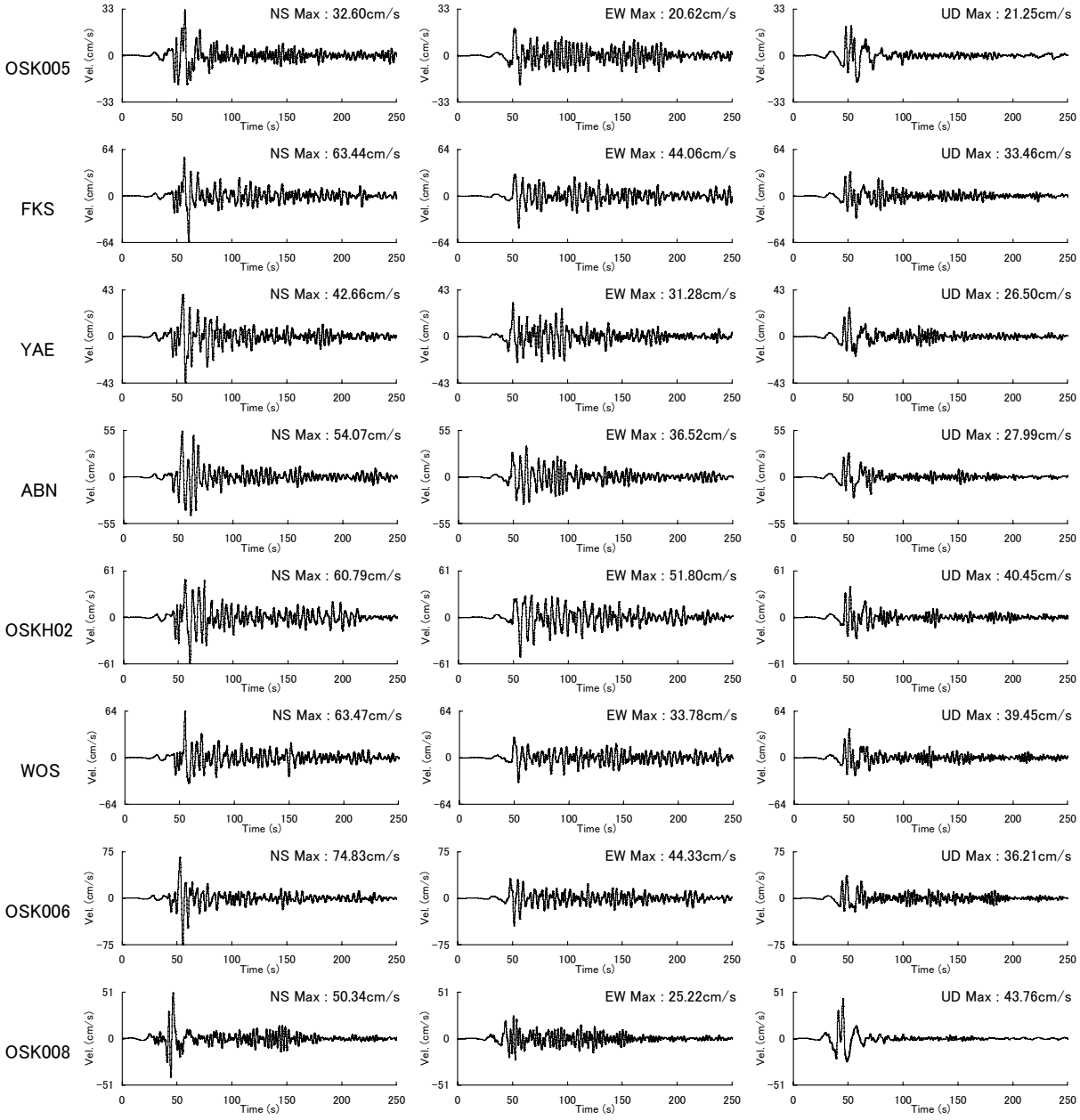

Figure 5 Synthesized velocity ground motion (0.05–0.4 Hz).

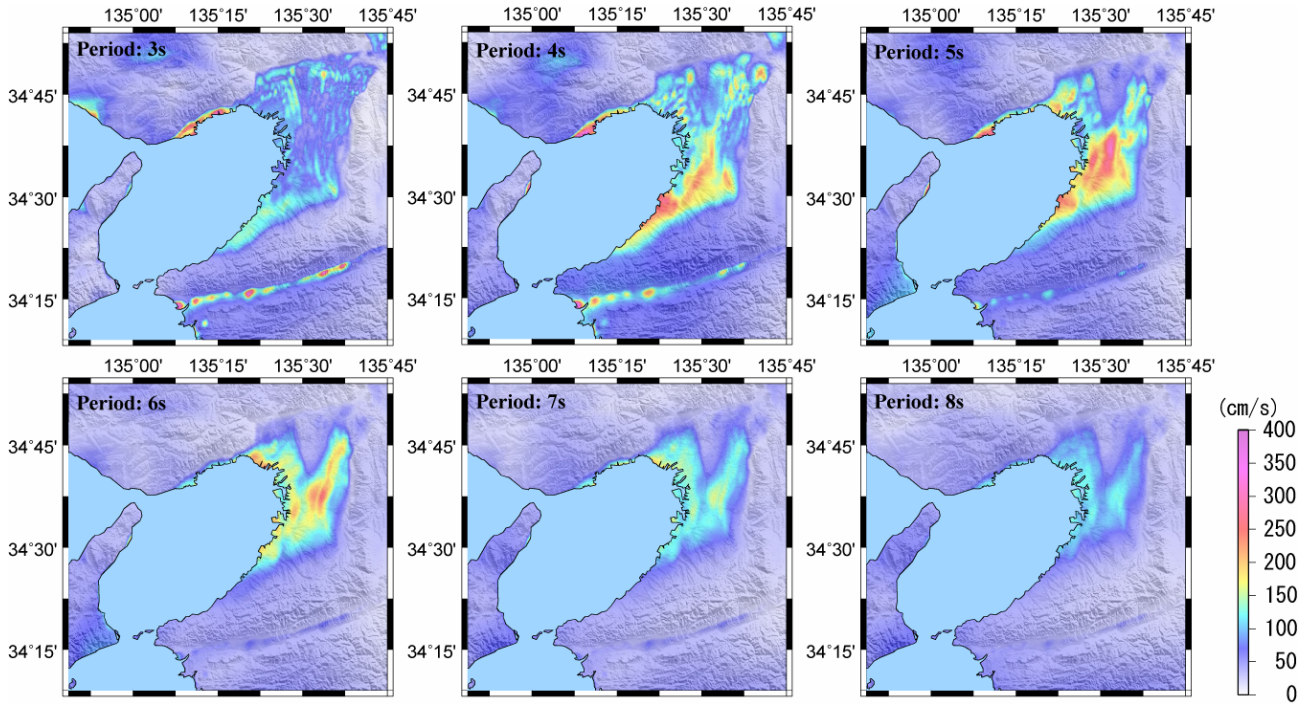

(a) NS component

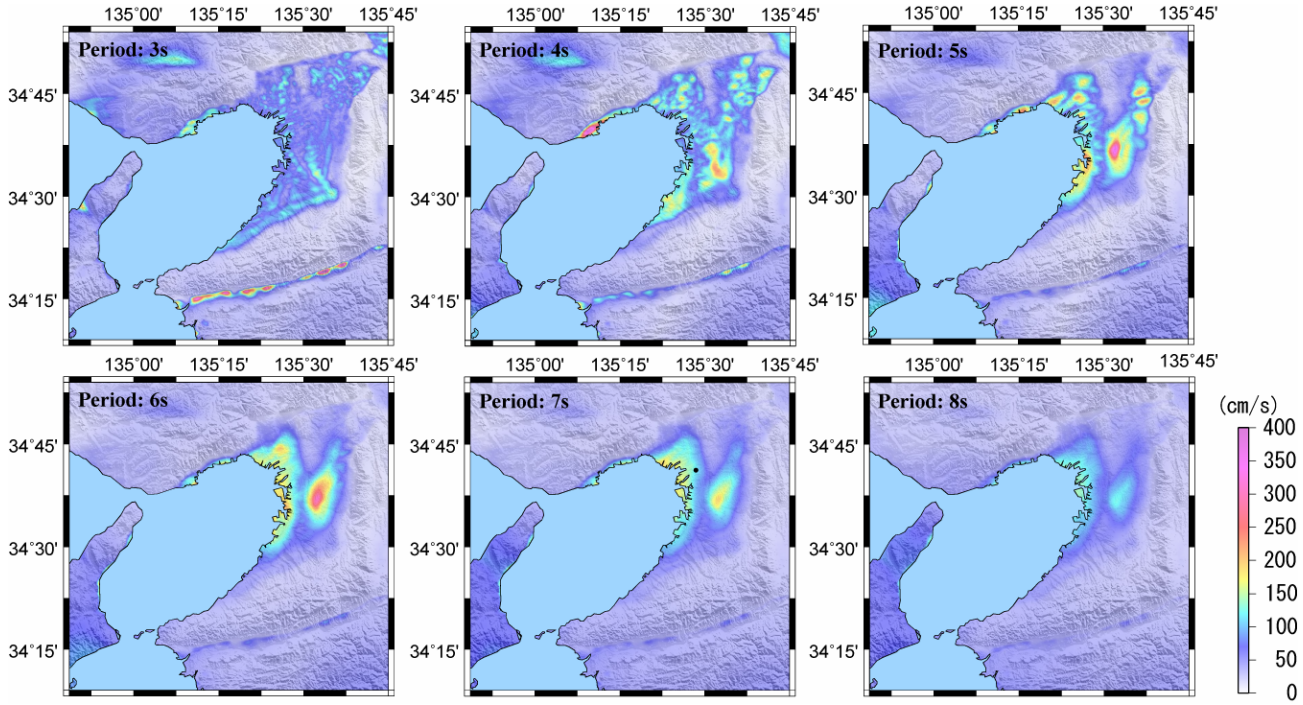

(b) WE component

Figure 6 Distributions of pseudo velocity response spectral amplitudes of the predicted ground motions for the Nankai earthquake in the Osaka basin (damping factor: 5%).

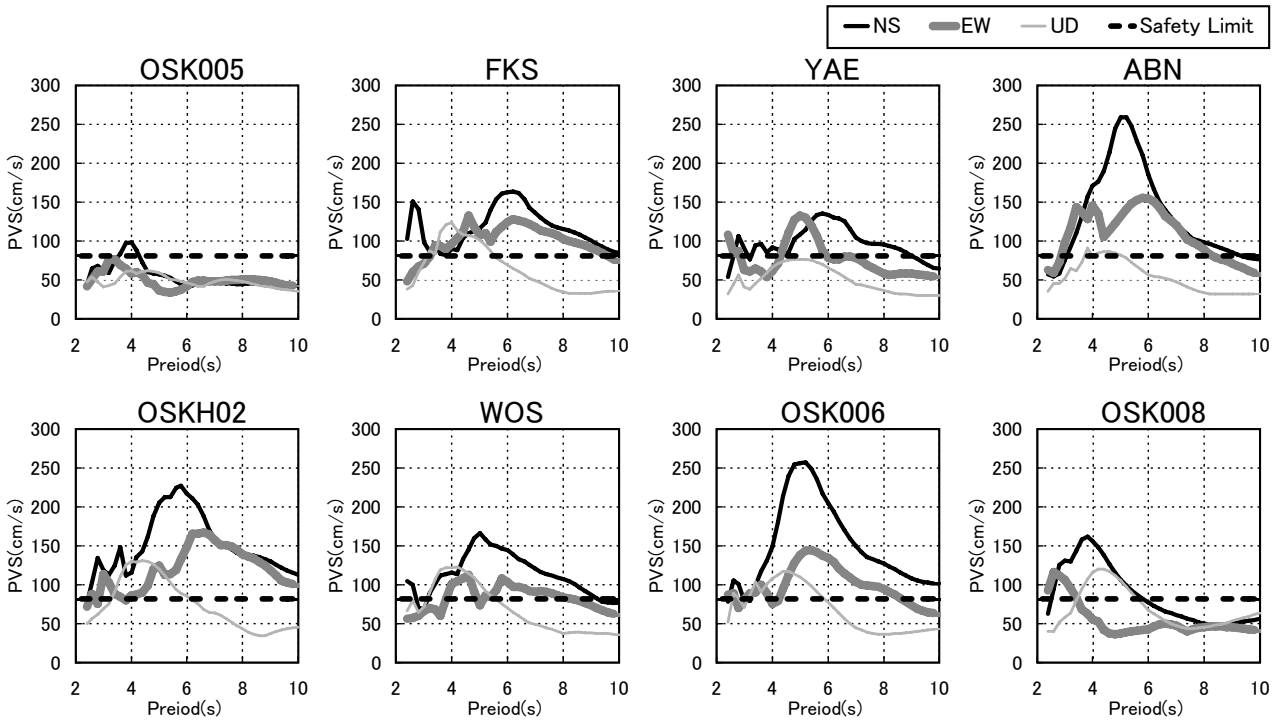

Figure 7 Pseudo velocity response spectra with 5% damping ratio and the safety limit level of the building design criterion in Japan. The safety limit level is defined for horizontal components at the engineering bedrock surface.

4. CONCLUSIONS

In this study, we predicted the long-period ground motions from the next Nankai earthquake, and showed the characteristics of the predicted long-period ground motions in the Osaka area. Furthermore, we discussed the possibility of earthquake damage from the predicted long-period ground motions. The largest peak ground velocities (PGVs) exceed 80 cm/s inside the Osaka basin during both earthquakes. The durations of the waveforms are longer than 4 min. The PGV distributions inside the Osaka basin drastically change depending on the incident directions of the seismic waves in the basin with complicated underground structure. The areas with relative larger amplitude extend along the northern as well as southern basin edges during the next Nankai earthquake. The predominant period of the predicted long-period ground motions is 4 to 6 s in the Osaka area, and the response spectral levels are beyond the safety limit level in building design regulation in Japan. These results indicate the possibility of earthquake damage in large-scale constructions due to the expected long-period ground motions. However, the current results are preliminary and should be revised using more accurate 3D underground structure models and different source scenarios. In particular, it is very important to know to what extent the predicted long period ground motions vary with plausible source parameters. We show the damage prediction map of high-rise buildings in the Osaka basin, using these long-period ground motions, in our other paper (Part 2).

ACKNOWLEDGMENTS

This work is supported by the Grant-in-Aid for Scientific Research (Basic Research (B), Grant No. 17310108) and by the Special Project for Earthquake Disaster Mitigation in Urban Areas from the Ministry of Education, Culture, Sports, Science and Technology of Japan.

REFERENCES

Cerjan, C., D. Kosloff, R. Kosloff and M. Reshef (1985). A nonreflecting boundary condition for discrete acoustic and elastic wave equations. *Geophysics* **50**, 705-708.

Clayton, R and B. Engquist (1977). Absorbing boundary conditions for acoustic and elastic wave equations. *Bull. Seism. Soc. Am.* **67**, 1529-1540.

Graves, R. W. (1996). Simulating seismic wave propagation in 3D elastic media using staggered-grid finite differences. *Bull. Seism. Soc. Am.* **86**, 1091-1106.

Hori, T., N. Kato, K. Hirahara, T. Baba and Y. Kaneda (2004). A numerical simulation of earthquake cycles along the Nankai Trough in southwest Japan: lateral variation in frictional property due to the slab geometry controls the nucleation position. *Earth and Plan. Sci. Lett.* **228**, 215-226.

Horikawa, H., K. Mizuno, T. Ishiyama, K. Satake, H. Sekiguchi, Y. Kase, Y. Sugiyama, H. Yokota, M. Suehiro, T. Yokokura, Y. Iwabuchi, N. Kitada and A. Pitarka (2003). A three-dimensional model of the subsurface structure beneath the Osaka sedimentary basin, southwest Japan, with fault-related structural discontinuities. *Annual Report on Active Fault and Paleoearthquake Researches, Geological Survey of Japan/AIST* **3**, 225-259. (in Japanese with English abstract)

Irikura, K., H. Miyake, T. Iwata, K. Kamae, H. Kawabe and L. A. Dalguer (2004). Recipe for predicting strong ground motions from future large earthquakes. 13th World Conference of Earthquake Engineering, Vancouver, Canada, Paper No. 1371.

Kagawa, T., S. Sawada, Y. Iwasaki and A. Nanjo (1993). Modeling of deep sedimentary structure of the Osaka Basin. *Proc. 22nd JSCE Earthq. Eng. Symp.*, 199-202. (in Japanese with English abstract)

Kawabe, H. and K. Kamae (2008). Prediction of long-period ground motions from huge subduction earthquakes in Osaka, *Japan. Journal of Seismology* **12:2**, 173-184.

Miyake, H. and K. Koketsu (2005). Long-period ground motions from a large offshore earthquake: The case of the 2004 off the Kii peninsula earthquake, Japan. *Earth Planets and Space* **57**, 203-207.

Miyakoshi, K., T. Kagawa, B. Zhao, T. Tokubayashi and S. Sawada (1999). Modeling of deep sedimentary structure of the Osaka Basin (3). *Proc. 25th JSCE Earthq. Eng. Symp.*, 185-188. (in Japanese with English abstract)

Nakamura, H. and T. Miyatake (2000). An approximate expression of slip velocity time function for simulation of near-field strong ground motion. *J. Seism. Soc. Japan* **53**, 1-9. (in Japanese with English abstract)

Nakanishi, A., H. Shiobara, R. Hino, K. Mochizuki, T. Sato, J. Kasahara, N. Takahashi, K. Suyehiro, H. Tokuyama, J. Segawa, M. Shinohara and H. Shimahura (2002). Deep crustal structure of the eastern Nankai trough and Zenisu ridge by dense airgun-OBS seismic profiling. *Mar. Geology* **187**, 47-62.

Nishimura, S., M. Ando and S. Miyazaki (1999). Inter-plate coupling along the Nankai Trough and southeastward motion along southern part of Kyushu. *J. Seism. Soc. Japan* **51**, 443-456. (in Japanese with English abstract)

Pitarka, A. (1999). 3D elastic finite-difference modeling of seismic wave propagation using staggered grid with non-uniform spacing. *Bull. Seism. Soc. Am.* **89**, 54-68.

Somerville, P., K. Irikura, R. W. Graves, S. Sawada, D. Wald, N. Abrahamson, Y. Iwasaki, T. Kagawa, N. Smith and A. Kowada (1999). Characterizing crustal earthquake slip models for the prediction of strong ground motion. *Seism. Res. L.* **70**, 59-80.

Yamada, N. and T. Iwata (2005). Long-period ground motion simulation in the Kinki area during the M_J 7.1 foreshock of the 2004 off the Kii peninsula earthquakes. *Earth Planets and Space* **57**, 197-202.

Zaho, S. and S. Takemoto (2000). Deformation and stress change associated with plate interaction at subduction zones: a kinematic modeling. *Geophys. J. Int.* **142**, 300-318.

Chapter 5: Damage Prediction of Long-Period Structure during Subduction Earthquakes –Part1: Prediction of Damage of High-Rise Buildings in the Osaka Basin for Future Nankai Earthquakes -

Damage prediction of long-period structures during subduction earthquakes Part2：Prediction of damage to high-rise buildings in the Osaka basin in future Nankai earthquakes

Yoshihisa NAKAGAWA[1], Katsuhiro KAMAE[2] , Hidenori KAWABE[3] and Kojiro IRIKURA[4]

1 Yasui Architects & Engineers Inc. ,Osaka, Japan

2 Professor, Research Reactor Institute, Kyoto University ,Osaka, Japan

3 Assistant Professor, Research Reactor Institute, Kyoto University ,Osaka, Japan

4 Professor, Disaster Prevention Research Center, Aichi Institute of Technology ,Toyota, Japan

Email: ynakagwa@yasui-archi.co.jp, kamae@kuca.rri.kyoto-u.ac.jp, kawabe@rri.kyoto-u.ac.jp, irikura@geor.or.jp

ABSTRACT :

High-rise buildings in mega-cities such as Osaka and Nagoya in Japan have a high probability of damage due to strong long-period ground motions from a great subduction earthquake. We predict the damage potential of steel and reinforced concrete high-rise buildings and construct damage prediction maps for the Osaka basin using the long-period ground motions of future Nankai earthquakes predicted in our other paper (Part 1). In this study, a one mass model (an analytical model for the equivalent mass of one degree of freedom) is adopted due to the need for a great deal of earthquake response analysis. We have confirmed through both earthquake observation and analytical results regarding high-rise buildings that the displacement and earthquake input energy of high-rise buildings subjected to long-period ground motion can be approximately estimated by this simple model. Using damage prediction maps, we point out that the dynamic response of high-rise buildings exceeds the present seismic design criteria in wide areas inside the Osaka basin.

KEYWORDS: Long-period ground motion, Nankai earthquake, Osaka basin, High-rise building, One mass model, Damage prediction map

1. INTRODUCTION

If a great subduction earthquake with the magnitude 8 class (Tonankai/Nankai earthquake) occurs, there is an extremely high probability that large metropolitan areas such as Osaka and Nagoya, which are located on large sedimentary basins, will be struck by long-period ground motions typical of massive earthquakes. Long-period structures such as high-rise buildings, seismic isolated structures, large bridges and oil tanks are concentrated in mega-cities, and face unprecedented earthquake damage due to long-period ground motions.

In this research, we attempted to create damage maps limited to high-rise buildings (steel or reinforced concrete) using predicted long-period ground motions in the Osaka basin during a Nankai earthquake, given in Part 1. Since earthquake response analysis of buildings had to be conducted for an extremely high number of points (the Osaka basin being divided into a 1km mesh), we adopted the simplest one mass model as the analysis model.

First, we use actual observations to verify the validity of the assumption of the one mass model—i.e. that high-rise buildings vibrate almost entirely in the first mode in response to long-period ground motions. Next, we analyze responses to long-period ground motion of a frame model and one mass model with regard to a high-rise building model, and show that displacement and earthquake input energy of high-rise buildings can be approximately estimated using the one mass model. Based on the above, and using a response analysis method for the one mass model, we then create damage maps for steel and reinforced concrete high-rise buildings with respect to predicted long-period ground motions at each point of the Osaka basin during a Nankai earthquake.

2. EARTHQUAKE OBSERVATION RESULTS AND SIMULATION ANALYSIS FOR HIGH-RISE BUILDINGS

Here we introduce an observation where a high-rise building vibrated almost entirely in the first mode in response to actual long-period ground motions. In the Kii Hanto Nanto Oki earthquake on September 5, 2004 (magnitude 7.4), long-period ground motions were observed at various points in the Osaka basin. Fig. 1 shows the EW component of acceleration records at the B2 and top 23rd floors of a 116m high steel high-rise building located in the eastern Osaka basin. Major shaking of the top floor continued for over 2 minutes, and this was due to long-period ground motions with a predominant period close to 6 seconds, as indicated by the velocity response spectrum of acceleration records for the lowermost floor (B2 floor) in Fig. 2.

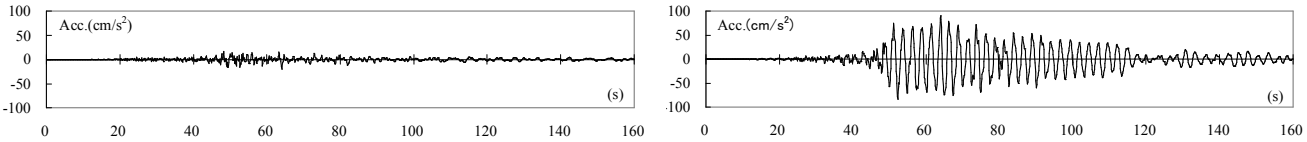

(a) B2 floor (EW) (b) 23th floor (EW)

Figure 1 Acceleration records

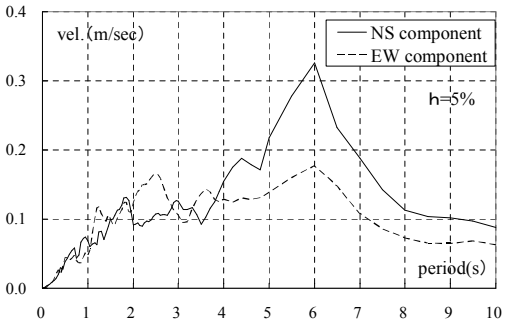

Figure 2 Velocity response spectrum of earthquake records at B2 floor

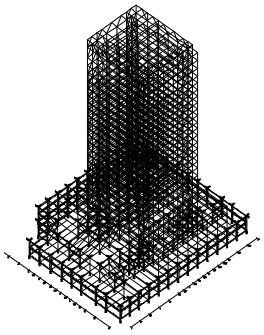

Figure 3 Frame model

Earthquake response analysis in the EW direction was conducted by replacing this building with the frame model shown in Fig. 3, and using the acceleration records as the input motion. Fig. 4 shows the acceleration time history at 23rd floor—both the observation records and analysis results using the frame model. The analysis results almost reproduce the observation records.

A one mass model with the same natural period (2.53 seconds) and damping ratio (1%) as the frame model was created, and a comparative analysis of the two models was done. If it is assumed that the building vibrates in the first mode, then the building displacement $\{D\}$ is determined according to Eqn.2.1 by the first participation vector $\{u_1\}$ and displacement of the one mass model $\overline{D}$. In this case, the displacement of the one mass model $\overline{D}$ corresponds to displacement of the building position where the participation vector for the first mode is 1.0 (hereafter this is called "typical point displacement").

$$\{D\} = \{u_1\}\overline{D} \tag{2.1}$$

Fig. 5 shows the displacement time history of the typical point (corresponding to the 17th floor) of the frame model in the EW direction, together with displacement $\overline{D}$ of the one mass model. The one mass model exhibits almost the same values as the frame model. Next, the maximum displacement ${}_iD_{max}$ and maximum story drift angle ${}_iR_{max}$ of each floor were estimated by the following equation using the maximum displacement of the one mass model $\overline{D}_{max}$, ${}_iu_1$ and story height H_i.

$$ {}_iD_{max} = {}_iu_1 \, \overline{D}_{max} \quad (2.2) $$

$$ {}_iR_{max} = ({}_{i+1}D_{max} - {}_iD_{max})/H_i \quad (2.3) $$

Fig. 6 shows results estimated using the one mass model together with results for the frame model, and there is a good correspondence between the two. The above results suggest that this building vibrated almost entirely in the first mode in response to long-period ground motion.

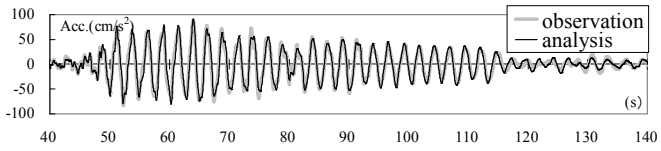

Figure.4 Observation records and analysis results using the frame model (Acceleration time history at 23rd floor)

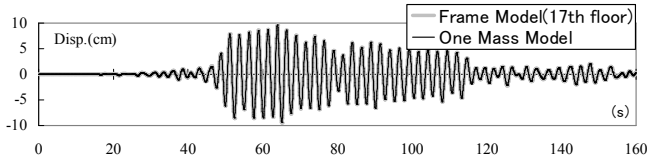

Figure.5 Displacement time history of both frame model (17th floor) and one mass model

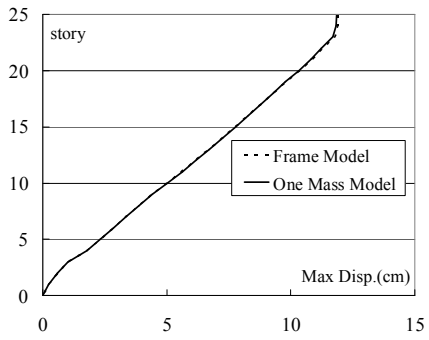

(a) Maximum displacement

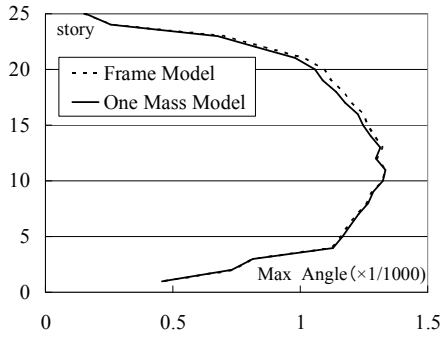

(b) Maximum story drift angle

Figure.6 Comparison of results using one mass model with results for frame model

3. DAMAGE INDICES OF HIGH-RISE BUILDING OBTAINED FROM RESPONSE PREDICTION USING THE ONE MASS MODEL

Generally when the first natural period of a buildings is in or less than the predominant period range of ground motion, the building will vibrate almost entirely in the first mode as shown in the preceding section. In particular, since we use the predicted long-period ground motions whose effective periods are longer than 2.5 seconds in this study, there is little possibility of higher modes being dominant even in high-rise buildings, given the assumption that the second natural period of buildings is nearly one third of the first natural period.

A building model was used to examine the degree to which response to long-period ground motions can be understood with a one mass model. The frame model for 82m high, 20 story steel building [2] shown in Fig. 7 was replaced with a one mass model, and a comparative analysis with the frame model was done in the Y direction (the first natural period 2.75 seconds). Fig. 8 shows the velocity response spectrum of the input motion, selected from the predicted ground motions in Part 1. With the one mass model, a building can be expressed with three parameters: the first natural period, yield base shear coefficient and damping ratio. We set the equivalent mass ratio for the first mode to 0.78, the damping ratio to 2%, and the yield base shear coefficient to 0.191. The hysteretic characteristic was set to be the normal bilinear model.

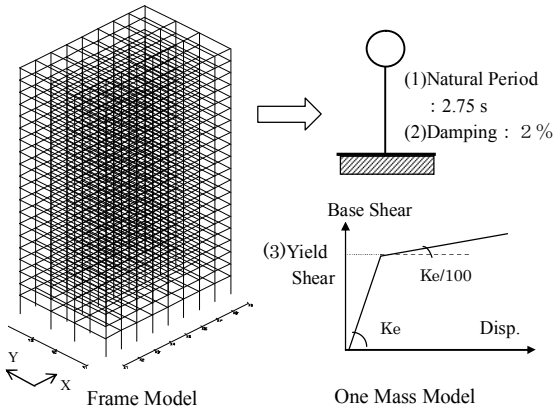

Figure.7 Frame model and one mass model for 20 story steel building

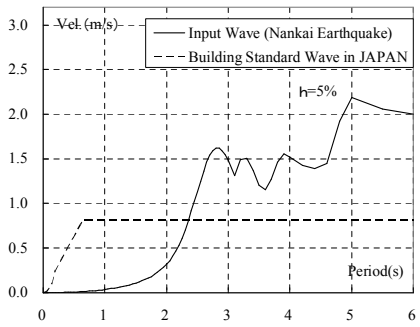

Figure.8 Velocity response spectrum of the input motion

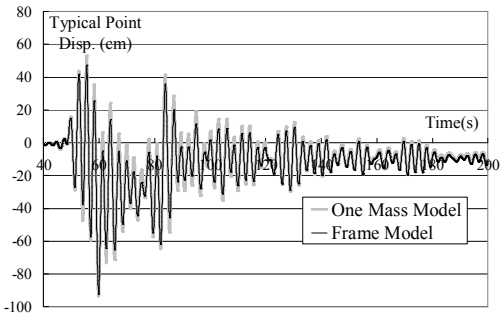

Figure.9 Displacement time history at building typical point

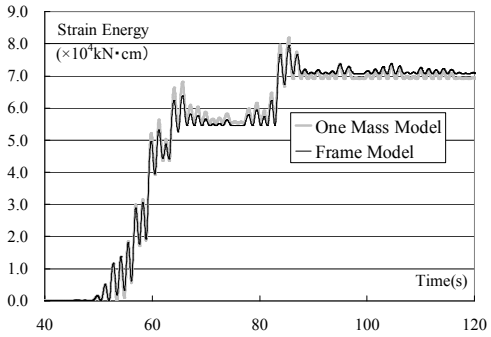

Figure.10 Time history of input energy contributing to damage (E_D)

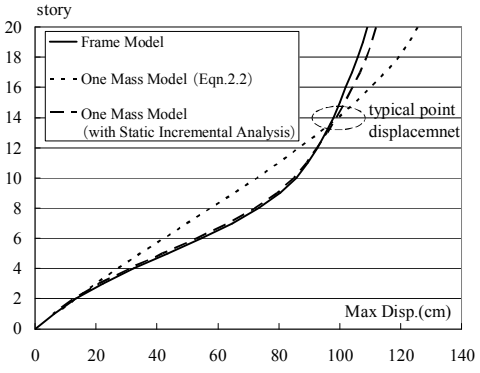

Figure.11 Maximum displacement

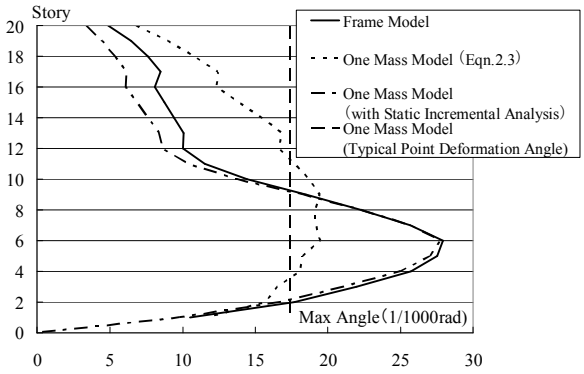

Figure.12 Maximum story drift angle

Figs. 9 and 10 show the time history of the typical point displacement and the total strain energy of beam and column members (hereafter called "input energy contributing to damage (E_D)"). For both response values, there is a good correspondence of the results for the one mass model and frame model. Figs. 11 and 12 show the maximum displacement and maximum story drift angle for each floor. The results for the one mass model, found using Eqn.2.2 and Eqn.2.3, are not greatly different from results for the frame model. This is because the displacement of each building floor depends on the relative relationship of the bearing strength distribution and external force distribution in the height direction of the building when the building enters the nonlinear domain. Thus, a static increment analysis was conducted taking the external force distribution as an Ai-distribution of the Japanese code, and the displacement and story drift angle for each floor, at the time when the typical point

displacement becomes the maximum displacement of the one mass model ($\bar{D}_{max}$), were shown in the same diagrams. There is a good correspondence with results for the frame model. Frame response results can be enough estimated even in the strongly nonlinear domain if static increment analysis is also used for analysis of the one mass model in this way. The maximum deformation angle of the building's typical point obtained from the one mass model $\bar{R}_{max}$(=maximum displacement of one mass model / building typical point height), is also indicated with a dotted line in Fig. 12. $\bar{R}_{max}$ shows almost the average value of each story drift angle and the difference with the maximum story drift angle increases when deformation is concentrated at a specific floor.

In this paper, the following three characteristics are used as high-rise building damage indices obtained from above analysis of the one mass model.

(a) Maximum building typical point displacement ($\bar{D}_{max}$)
(b) Maximum deformation angle of building typical point ($\bar{R}_{max}$)
(c) Velocity converted value of input energy contributing to damage E_D (V_D)

In the Japanese seismic design method based on energy balance, the design value V_D ($=\sqrt{2E_D/M}$) for buildings on medium class ground is required to be 165cm/s. Using this design method based on V_D, it is possible to calculate the necessary cumulative plastic deformation of beam and column members at each story [4].

4. DAMAGE PREDICTION FOR HIGH-RISE BUILDINGS IN THE OSAKA BASIN

4.1 Analysis model

Prediction of damage to steel and reinforced concrete high-rise buildings is done using the one mass model indicated below.

The hysteretic characteristic is set to the normal bilinear model for steel, and to the degrading trilinear model for reinforced concrete as shown in Fig. 13. Q_u in Fig. 13 is calculated using the yield base shear coefficient C_u given by Eqn.4.1, where C_1 is the base shear coefficient for the allowable stress design and is generally expressed by the first natural period T_1. That is C_1= 0.3/T1 for steel and C_1= 0.18/ T_1 for reinforced concrete [3]. Multiplier β is normally in the range 1.5–2.5. In the skeleton curve for reinforced concrete, we set Q_c/Q_u to 0.17 and K_y/K_e to 0.41, assuming a standard structure consisting of beam and column members.

$$C_u = \beta\ C_1 \qquad (4.1)$$

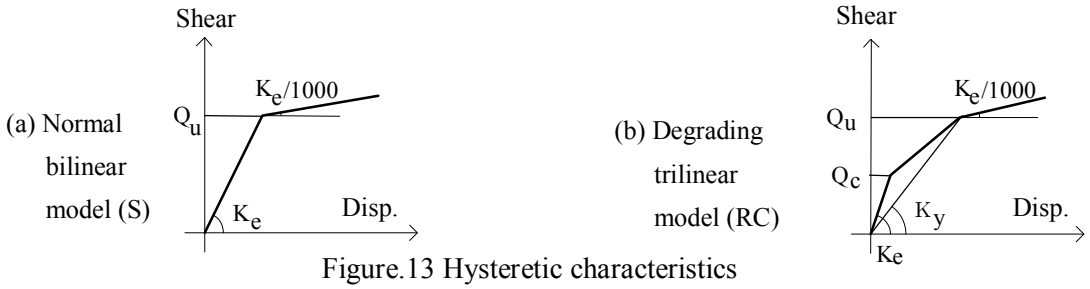

Figure.13 Hysteretic characteristics

The equivalent mass ratio is taken to be 0.78, assuming that the distribution of mass is uniform in height and the story drift angles of each floor are the same for external force with an Ai-distribution of the Japanese code. We use initial stiffness proportional damping with the first damping ratio set to 2% for steel, and instantaneous

stiffness proportional damping with the first damping ratio set to 3% for reinforced concrete. The height of the building typical point H_1 necessary for calculating $\bar{R}_{max}$ is found from the building height H and the participation factor for the first mode α (= 1.37), where H is generally expressed by T_1, that is $H = T_1/0.026$ for steel and $H = T_1/0.019$ for reinforced concrete [3].

4.2 Damage map for high-rise buildings

We conducted earthquake response analysis based on the one mass model for predicted ground motions at each point in the Osaka basin. Using the damage indices obtained from the above analysis, we constructed damage prediction map for high-rise buildings with natural periods of 3 to 6 seconds for steel and 2 to 5 seconds for reinforced concrete.

Figs. 14–16 show damage maps for $\bar{D}_{max}$, $\bar{R}_{max}$ and V_D of steel and reinforced concrete high-rise buildings with one second increment of natural periods. We used ground motions for the NS component whose maximum velocity is larger than the EW component at most points as shown in Part 1, and β in Eqn.4.1 is 2.0, which is an average value of building bearing strength. The following points can be noted from these earthquake damage maps.

(1) There are many regions where the maximum deformation angle of the typical point $\bar{R}_{max}$, which indicates the average value of the story drift angles for each story, exceeds the design criteria (1/100) for the story drift angle of a high-rise building, and regions where the velocity converted value V_D of the input energy contributing to damage exceeds the design criteria (165cm/s) for buildings on medium class ground. If there are high-rise buildings with the pertinent natural period in these regions, it would be desirable to conduct more detailed studies in the future.

(2) Regions where there is large deformation of steel high-rise buildings are: the Kobe coast for buildings with a natural period of 3 seconds, the Kobe coast and southern Osaka for buildings with a period of 4 seconds, and almost everywhere except southern Osaka for buildings with a period of 5 or 6 seconds. Large earthquake energy is input over a wide range of the Osaka basin particularly for buildings with a period of 5 or 6 seconds.

(3) Regions where there is large deformation of reinforced concrete high-rise buildings are: the Kobe coast for buildings with a natural period of 2 seconds, the Kobe coast and the central/southern Osaka basin for buildings with a period of 3 seconds, and almost everywhere except southern Osaka for buildings with a period of 4 or 5 seconds. Large earthquake energy is input over a wide range of the Osaka basin for buildings with a period of 3 or 4 seconds. Reinforced concrete buildings enter the nonlinear domain quickly due to cracking of concrete, and thus input energy contributing to damage is greater than for steel buildings.

5. CONCLUSION

Focusing on the Osaka basin, where there is a high probability of being struck by strong long-period ground motions in the case of a potential Nankai earthquake (M8.4), we have created damage maps for steel and reinforced concrete high-rise buildings, and shown that story drift angles and earthquake energy inputs exceeding the present design criteria can potentially occur over a wide range, depending on the building natural period band. This applies in particular to steel buildings with a first natural period of 5 to 6 seconds, and reinforced concrete buildings with a period of 4 to 5 seconds. With the ground motion for design of high-rise buildings in current Japanese building code, the characteristics of the subsurface ground are taken into account as site characteristics, but there is no consideration of the characteristics of deep ground structures, which are closely related to the period band (longer than 2.5 seconds) of the predicted long-period ground motions used in

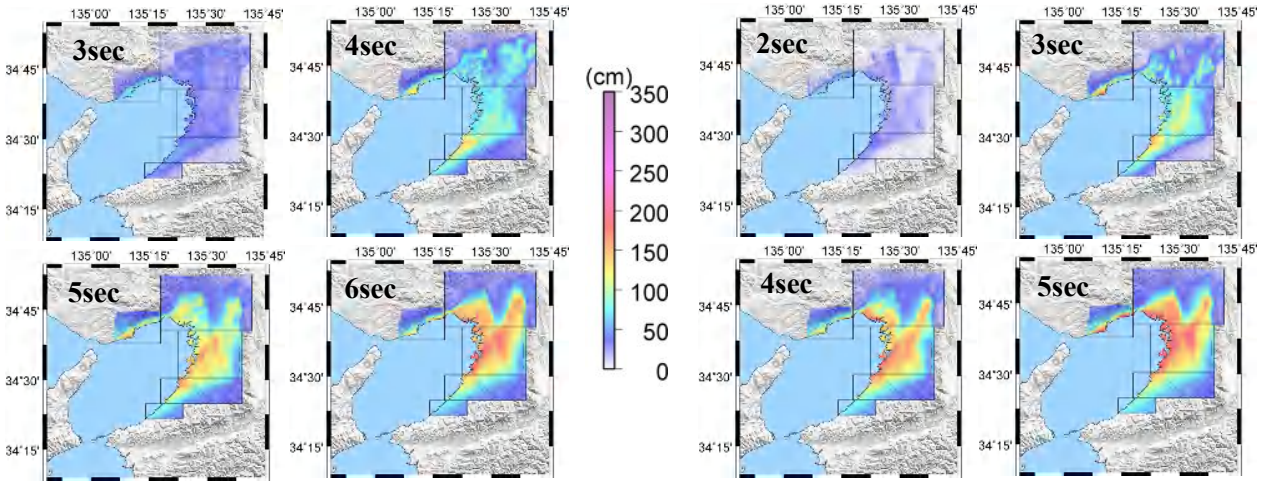

(a) Steel structure (b) Reinforced concrete structure

Figure.14 Maximum Building typical point displacement $\overline{D}_{max}$

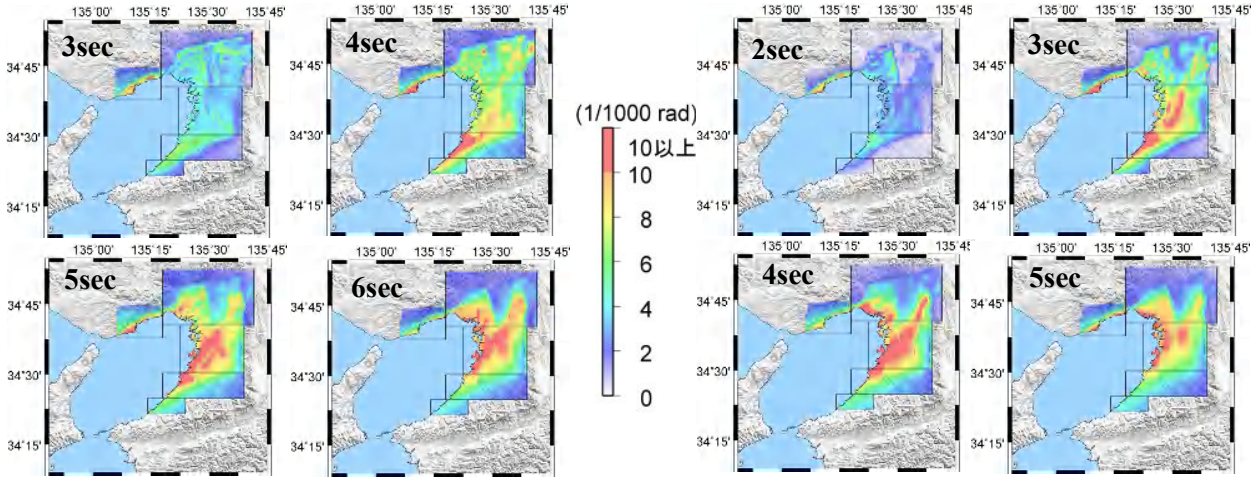

(a) Steel structure (b) Reinforced concrete structure

Figure.15 Maximum Deformation angle of building typical point $\overline{R}_{max}$

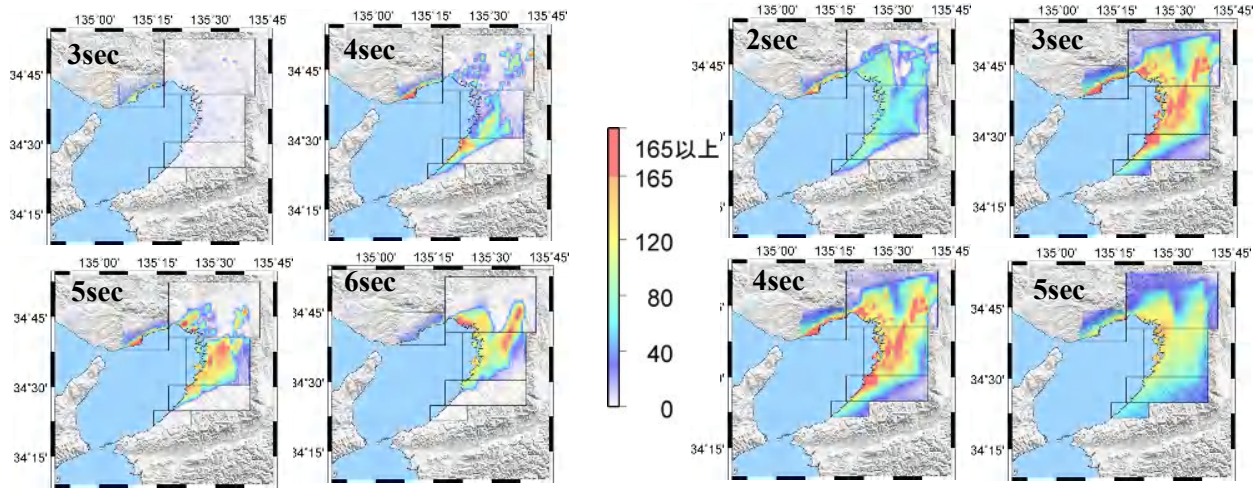

(a) Steel structure (b) Reinforced concrete structure

Figure.16 The velocity converted value V_D of input energy contributing to damage

this research. In the Osaka basin, where dominance in a longer period band is predicted in a Nankai earthquake or other massive earthquake, there is a need to examine the seismic safety of high-rise buildings using predicted ground motions which also take into account deep ground structures.

When predicting damage over a wide area to long-period structures due to long-period ground motions, the technique based on a one mass model given here is useful for easily developing an understanding of the general situation. If some basic information regarding an individual building is known—i.e. building position, structural type, natural period, yield base shear coefficient—then it is possible to roughly understand the building's average story drift angle and input energy contributing to damage from the damage map. It is also possible to estimate the maximum story drift angle of each floor by conducting static increment analysis of the building up to the index $\bar{D}_{max}$. The necessary cumulative plastic deformation of beam and column members can be approximately estimated from the index V_D by using the calculation technique based on energy balance.

The uncertainty of the characteristics of buildings and predicted ground motions cannot be denied in predicting earthquake damage to buildings. The damage maps presented here apply to high-rise buildings having average restoring force characteristics and damping characteristics, and the assumed Nankai earthquake is based on a single scenario. Damage maps based on a one mass model can be created comparatively easily, and thus in the future we plan to apply this technique to different characteristics of buildings and multiple scenario earthquakes, and examine the resulting effects. Also, this study focused on long-period ground motions of 2.5 seconds or longer, and future studies will need to look at a wider band of predicted ground motions, and take into account the higher order modes of high-rise buildings.

ACKNOWLEDGEMENTS

This research was conducted based on a Grant-in-Aid for Scientific Research, Basic Research (B) (Grant no.: 17310108). In preparing this manuscript, valuable comments were received from the grant recipient and other collaborators, and the authors would like to express their gratitude.

REFERRENCES

1.Comartin, C., R.Niewiarowski and C.Rojahm (1996). Chapter 8 Nonlinear static analysis procedures, ATC-40 Seismic evaluation and retrofit of concrete buildings Volume 1, Applied Technology Council.
2.Sekiya, E., H.Mori, T.Ohbuchi, K.Yoshie, H.Hara, F.Arita., Y.Takeuchi, I,Y.Saito, M.Ishii, and K.Kasai (2004). Details of 4-,10-,& 2- story theme structure used for passive control design examples, *Passive Control Symposium 2004*, 263-278.
3.Kimura, U., S.Ichimura, T.Fukushima, and T.Teramoto (2000). Study on the mechanical feature of high-rise building, *Summaries of technical papers of Annual Meeting AIJ*, Structures 3, 865-866.
4.Hasegawa, T., I.Nishiyama, A.Mukai, T.Ishihara and H,Kamura (2004). Seismic response prediction of steel frames with hysteretic dampers based on energy balance, *Journal of structural and construction engineering, AIJ*, No582, 147-154.
5.Kawabe, H., K.Kamae and K.Irikura (2007). Damage prediction of long-period structures during great subduction earthquakes Part1: Long-period ground motion prediction in the Osaka basin for the future Nankai Earthquake, *Summaries of technical papers of Annual Meeting AIJ*, Structures 2, 415-416.
6.Nakagawa, Y., K.Irikura, K.Kamae and H.Kawabe (2007), Damage prediction of long-period structures during great subduction earthquakes Part2: Damage prediction map of steel high-rise buildings in the Osaka basin for the future Nankai Earthquake, *Summaries of technical papers of Annual Meeting AIJ*, Structures 2,417-418